Iron Overload Coordinately Promotes Ferritin Expression and Fat Accumulation in *Caenorhabditis elegans*

Haizhen Wang,*,†,1 Xue Jiang,*,†,1 Jieyu Wu,*,† Linqiang Zhang,*,† Jingfei Huang,‡ Yuru Zhang,* Xiaoju Zou,§,2 and Bin Liang*,2

*Key Laboratory of Animal Models and Human Disease Mechanisms of the Chinese Academy of Sciences and Yunnan Province, Kunming Institute of Zoology, Chinese Academy of Sciences, Kunming 650223, China, †Kunming College of Life Science, University of Chinese Academy of Sciences, Kunming, Yunnan 650204, China, ‡State Key Laboratory of Genetic Resources and Evolution, Kunming Institute of Zoology, Chinese Academy of Sciences, Kunming 650223, China, and §Department of Life Science and Biotechnology, Key Laboratory of Special Biological Resource Development and Utilization of University in Yunnan Province, Kunming University, Kunming 650214, China

ORCID ID: 0000-0001-9131-5478 (X.J.)

ABSTRACT The trace element iron is crucial for living organisms, since it plays essential roles in numerous cellular functions. Systemic iron overload and the elevated level of ferritin, a ubiquitous intracellular protein that stores and releases iron to maintain the iron homeostasis in cells, has long been epidemiologically associated with obesity and obesity-related diseases. However, the underlying mechanisms of this association remain unclear. Here, using *Caenorhabditis elegans*, we show that iron overload induces the expression of *sgk-1*, encoding the serum and glucocorticoid-inducible kinase, to promote the level of ferritin and fat accumulation. Mutation of *cyp-23A1*, encoding a homolog of human cytochrome P450 CYP7B1 that is related to neonatal hemochromatosis, further enhances the elevated expression of *ftn-1*, *sgk-1*, and fat accumulation. *sgk-1* positively regulates the expression of *acs-20* and *vit-2*, genes encoding homologs of the mammalian FATP1/4 fatty acid transport proteins and yolk lipoproteins, respectively, to facilitate lipid uptake and translocation for storage under iron overload. This study reveals a completely novel pathway in which *sgk-1* plays a central role to synergistically regulate iron and lipid homeostasis, offering not only experimental evidence supporting a previously unverified link between iron and obesity, but also novel insights into the pathogenesis of iron and obesity-related human metabolic diseases.

KEYWORDS iron; serum and glucocorticoid inducible kinase SGK-1; lipid uptake; obesity; *C. elegans*

DUE to its essential roles in numerous cellular functions across nearly all living organisms, including oxygen transport, electron transport, DNA synthesis, and enzyme catalysis, exploring how iron is stored and regulated has been a growing focus in numerous fields. Dietary iron is absorbed primarily by duodenal enterocytes via the divalent metal-ion transporter 1 (DMT1) after it is reduced at the apical membrane. Subsequently, it is either stored in ferritin, which dynamically regulates iron sequestration, storage, and release or it is transported from enterocytes into the blood stream via the basolateral transporter ferroportin (Fleming and Ponka 2012). Consequently, the total amount of iron in the body is determined by its intake and storage, which are all finely regulated by many factors and signaling pathways at various levels (Fleming and Ponka 2012; Hubler *et al.* 2015), many of which not entirely understood.

Human epidemiology studies revealed that elevated levels of ferritin may be an indication of systemic iron overload (Cook *et al.* 1974; Zimmermann 2008) and are positively associated with obesity (Wenzel *et al.* 1962; Gillum 2001; Iwasaki *et al.* 2005) and obesity-related diseases such as diabetes, hypertension, dyslipidaemia, or nonalcoholic fatty

Copyright © 2016 by the Genetics Society of America
doi: 10.1534/genetics.116.186742
Manuscript received January 4, 2016; accepted for publication March 20, 2016; published Early Online March 23, 2016.
Supplemental material is available online at www.genetics.org/lookup/suppl/doi:10.1534/genetics.116.186742/-/DC1.
[1]These authors contributed equally to this work.
[2]Corresponding authors: Kunming Institute of Zoology, 32 Jiaochangdonglu Rd., Kunming 650223, China. E-mail: liangb@mail.kiz.ac.cn; and Department of Life Science and Biotechnology, Key Laboratory of Special Biological Resource Development and Utilization of University in Yunnan Province, Kunming University, Kunming 650214, China. E-mail: xiaojuzou@163.com

liver disease (Jehn *et al.* 2004; Bozzini *et al.* 2005; Mascitelli *et al.* 2009; Dongiovanni *et al.* 2011; Kim *et al.* 2011; see Zafon *et al.* 2010 for review). Precisely why elevations in ferritin levels or systemic iron overload are associated with these conditions is not entirely clear, with potential explanations ranging from excess iron causing oxidative stress, endoplasmic reticulum (ER) stress, inflammation, and dysfunction of adipose tissue (Hubler *et al.* 2015; Nikonorov *et al.* 2015).

When including other environmental or dietary factors, the relationship between obesity, its comorbidities, and iron becomes more complex. Iron is required for the adipogenesis of the 3T3-L1 preadipocytes (Moreno-Navarrete *et al.* 2014a), and it increases the rate of adipocyte lipolysis (Rumberger *et al.* 2004). In the mouse liver, iron significantly upregulates the transcripts of seven enzymes in the cholesterol biosynthesis pathway, resulting into cholesterol accumulation. This occurs independently of the conserved lipogenic regulator SREBP2 (Graham *et al.* 2010). The combination of iron and lipid-rich diet may exacerbate this situation because lipids also cause oxidative and ER stress, as well as inflammation. Collectively, this helps explain why dietary iron supplementation concurrent with a high-fat diet (HFD) greatly increases adiposity in rats (Tinkov *et al.* 2013), as well as hepatic fat accumulation in the liver of mice (Choi *et al.* 2013). The association seems to also hold true in reverse. Several studies found that reduction of iron by several different methods led to amelioration of adiposity and improvement of obesity and obesity-related diseases (Zhang *et al.* 2005; Fleming and Ponka 2012; Tajima *et al.* 2012; Moreno-Navarrete *et al.* 2014a,b). Unfortunately, the mechanisms of this association between iron and lipid accumulation or obesity remain largely unclear.

Though human clinical studies would likely shed a great deal of light on this relationship, such studies are not always practical or even possible. Alternatively, *Caenorhabditis elegans* may offer an ideal model due to the highly conserved nature of many proteins involved in iron homeostasis, including iron uptake (SMF-3, a homolog of DMT1), storage (FTN-1 and FTN-2, encoding ferritin), and export (FPN-1.1, FPN-1.2, FPN-1.3, encoding ferroportin), as well as potential orthologs for DCYTB ferrireductase and hephaestin multicopper oxidase (Anderson and Leibold 2014). Moreover, *C. elegans* FTN-1 and FTN-2 are more similar to human FTH than to FTL, and both FTN-1 and FTN-2 contain ferroxidase active-site residues (Gourley *et al.* 2003). Under iron overload, the expression of *ftn-1* gene and protein, and to a lesser extent *ftn-2*, are induced; in contrast, the expression of SMF-3 is suppressed to reduce iron uptake (Gourley *et al.* 2003; Kim *et al.* 2004). *ftn-1* RNAi (Kim *et al.* 2004) or *ftn-1(ok3625)* deletion mutant (Valentini *et al.* 2012) are iron sensitive and have reduced lifespans when exposed to high iron.

While these studies have investigated how iron affects growth, development, and longevity in *C. elegans*, whether or not it also coordinately regulates lipid metabolism is entirely unclear. In this study, we used *C. elegans* to identify novel genes and unravel complex pathways involved in iron metabolism and lipid metabolism. Our results show that iron overload by the established dietary supplementation with ammonium ferric citrate (FAC) (Gourley *et al.* 2003) coordinately promotes the expression of ferritin and fat accumulation in *C. elegans*. Specifically, iron overload induces the serum and glucocorticoid-inducible kinase *sgk-1* to positively regulate *acs-20* and *vit-2*, facilitating lipid uptake and accumulation.

Materials and Methods

C. elegans strains

C. elegans strains were maintained under standard culture conditions on NGM agar with *Escherichia coli* OP50, unless otherwise specified. The wild-type strain was N2. The strains used in this study were as follows: *acs-20(tm3232)IV*, *age-1(hx546)II*, *akt-1(ok525)V*, *cyp-23A1(gk253)II*, *daf-2(e1370)III*, *ftn-1::GFP{XA6900*, *pha-1 (e2123ts)III;qaEx01[ftn-1::△pes-10::GFP-his, pha-1(+)]}* (Romney *et al.* 2008), *cyp-23A1(gk253)II;ftn-1::GFP{XA6900*, *pha-1(e2123ts)III;qaEx01[ftn-1::△pes-10 ::GFP-his, pha-1(+)]}*, *sgk-1(ft15)X*, *sgk-1(ok538)X*, *sgk-1(ok538)X;cyp-23A1(gk253)*, *sgk-1::gfp(MQD862, N2;Psgk-1::sgk-1::gfp [hqIs150]*) (Hertweck *et al.* 2004; Zhu *et al.* 2015), *rsks-1(ok1255)III*, *vit-2(ok3211)X*, *vit-3(ok2348)X*, *vit-2::gfp {RT130,unc-199(ed3);pwIs23[Pvit-2::vit-2::gfp, unc-199(+)]}* (Van Rompay *et al.* 2015), *cyp-23A1(gk253);vit-2::gfp {RT130*, *unc-199(ed3);pwIs23 [Pvit-2::vit-2::gfp,unc-199(+)]}*, and *acs-20(tm3232);vit-2::gfp {RT130,unc-199(ed3)*; *pwIs23[Pvit-2::vit-2::gfp,unc119(+)]}*.

Construction of Psgk-1::gfp extrachromosomal transgenic strain

The *Psgk-1*::*gfp* transgenes were created using methods as previously described by Frokjaer-Jensen *et al.* (2008), and the transgenic strain was created by microinjection. Briefly, an extrachromosomal transgenic strain was made by injection into the EG4322 (*ttTi5605;unc-119(ed3)*). The injection mix consisted of 50 ng/μl pCFJ151 inserted with target DNA fragment, pJL43.1 (*Pglh-2*::*transposase*), 5 ng/μl pCFJ104 (*Pmyo-3*::*mCherry*), and 2.5 ng/μl pCFJ90 (*Pmyo-2*::*mCherry*). DNA mixtures were injected into the gonads of young adult *C. elegans*. The extrachromosomal transgenic strain was assigned kun*Ex*126[*unc-119(ed3)*; *Psgk-1*::*gfp*+*unc-119*(+)]. The primers used for amplification of *Psgk-1*::*gfp* are *Psgk-1*F: GGATATCTGGATCCACGAA CTCCGGTAACTTACTCATTTTC and *Psgk-1*R2: GTCGACCTG CAGGCATGCAACC TCACCATTCTCGACTCTG; and GFP+*unc-54* 3′UTR-F: TTGCATGCCTGCAGGTCG AC and GFP+*unc-54* 3′UTR-R: CCAGAGCTCACCTAGGTATCTGCCGACTAGTAG GAAACAGT.

Supplementation of FAC

FAC supplementation was performed as described previously (Romney *et al.* 2008). In brief, synchronized L1 worms were placed and cultivated on NGM plates supplemented with

2.5 mg/ml or 5 mg/ml FAC. The pH value of FAC medium was adjusted to 7.0. L4 worms or young adults were harvested for further analysis.

RNAi screen regulators of ftn-1::GFP

Synchronized *ftn-1*::*GFP*(*XA6900*) L1 worms were seeded on NGM plates supplemented with FAC (5 mg/ml) or not. The performance of RNAi by feeding was followed as we described previously (Zhang *et al.* 2013). Worms were collected at ~60 hr, at young adult stage, and GFP fluorescence was visualized under a fluorescence microscope (BX53, Olympus). RNAi of a specific gene displaying changed expression of FTN-1::GFP was considered a potential regulator of *ftn-1*::*GFP*.

Visualization of GFP fluorescence

At least 20 GFP worms were picked and mounted on an agarose pad and anesthetized using 10 mM sodium azide. GFP fluorescence was visualized under an Olympus BX53 fluorescence microscope.

Quantitative PCR analysis

Total RNA and cDNA preparation and quantitative PCR (qPCR) performance were followed as described previously (Ding *et al.* 2015).

Nile Red staining of fixed nematodes

L4s or young adult nematodes were washed off of growth plates and then fixed and stained with Nile Red as done previously (Brooks *et al.* 2009; Liang *et al.* 2010). Images were captured using identical settings and exposure time for each image, unless specifically noted.

Lipid extraction and analysis

Lipid extraction and analysis of young adult nematodes was determined as described previously (Watts and Browse 2006; Shi *et al.* 2013). To determine the triacylglycerol (TAG) and phospholipids, lipid extraction, thin-layer chromatography (TLC), and gas chromatography (GC) were performed as described (Watts and Browse 2006; Shi *et al.* 2013).

Dietary supplementation of oleic acid [C18:1(n-9)]

Fatty acid supplementation was carried out by adding sodium oleic acid (OA) (NuChek Prep) at a final concentration of 0.2 mM to NGM media as we previously described (Shi *et al.* 2013). Synchronized L1 worms were cultivated on NGM agar plates supplemented with OA. Young adults were washed off the plates, and fatty acid composition of adult nematodes was determined as previously described (Watts and Browse 2002; Liang *et al.* 2010).

Fluorescent fatty acid probe analysis

Analysis of fluorescent fatty acid probe was modified from Spanier *et al.* (2009). The 4,4-difluoro-5-methyl-4-bora-3a,4a-diaza-3-indacene-dodecanoic acid (BODIPY 500/510 C1, C12; Sigma) was dissolved in DMSO to a final concentration of 2.4 μM and then attenuated to 20 nM by M9 buffer. Briefly, synchronized L1 worms were cultivated on NGM plates and harvested at L4 stage, then immediately incubated in 20 nM BODIPY-12 solution for 10 min, and then visualized under a fluorescent microscope (BX53, Olympus).

Quantification of lipid droplet size

Quantification of the diameter of lipid droplets (LDs) was followed as described by Shi *et al.* (2013). In brief, young adult worms were fixed and stained by Nile Red and photographed. A 50 × 50 μm square was selected in the middle of the intestine for each worm and all of the LDs in this square were measured by the software CellSens Standard (Olympus). Roughly 10 worms were measured for each worm strain or treatment.

Lipid droplet purification

LDs of *C. elegans* were isolated as described by Zhang *et al.* (2012). In brief, 4×10^5 worms were harvested and washed by M9 buffer three times, and by buffer A. Next, worms were homogenized by a homogenizer (Cole-Parmer LabGENR700) and centrifuged at 1000 × *g* for 30 sec. The supernatants were homogenized again by a nitrogen cell disruption vessel (4639 45-ml cell disruption vessel; Parr Instrument, Moline, IL) at 500 psi for 30 min on ice. A 9-ml supernatant was loaded into a sw40 tube with 3 ml buffer B on the top and centrifuged at 10,000 × *g* for 1 hr at 4°. The LD fraction was transferred to another 1.5-ml tube and washed with 200 μl buffer B three times.

Western blot analysis

Young adults with one to three eggs were harvested, and their tissues ground and homogenized at 4° with an extraction buffer. The tissue homogenates were then centrifuged, and the supernatants were used for Western blot analysis. The LD protein and lipid samples were prepared as previously described (Zhang *et al.* 2012). Proteins were separated by 12% SDS gel (Bio-Rad) and then transferred to polyvinylidene difluoride membranes. The primary antibodies were sc8334 (Santa Cruz Biotechnology) rabbit anti-GFP antibody at 1:200 dilution, O00141 (Enzo) rabbit anti-SGK-1 antibody at 1:1000 dilution. Anti-DHS-3, anti-CAV-1, and anti-BIP antibodies were used as previously described by Zhang *et al.* (2012). The secondary antibody was goat antirabbit IgG from Beyotime at 1:5000 dilution. The membrane was exposed to chemiluminescent substrate (Pierce), and the film (Carestream, Xiamen, China) was then developed.

Statistical analysis

Data are presented as mean ± SEM, except when specifically indicated. Statistical analysis performed included *t*-test or analysis of variance (ANOVA) followed by least significant difference multiple comparisons using SPSS20.0 (IBM SPSS Statistics, Armonk, NY). All figures were made using GraphPad Prism 5 (GraphPad Software, La Jolla, CA).

Data availability

The authors state that all data necessary for confirming the conclusions presented in the article are represented fully within the article.

Results

Iron induces sgk-1 expression to upregulate ferritin expression and fat accumulation

To determine whether iron overload promotes fat accumulation in *C. elegans*, we applied FAC to NGM plates. Consistent with previous reports (Gourley *et al.* 2003; Romney *et al.* 2008), FAC induced the expression of FTN-1::GFP (Figure 1A) and *ftn-1* messenger RNA (mRNA) (Figure 1B) in wild-type N2 . Concurrently, FAC promoted fat accumulation, as indicated by an increased size of LDs and increased abundance of large-sized LDs (Figure 1C and Supplemental Material, Figure S1, A and B, and Figure S2). Consistently, isolated LDs from N2 as well as two reported LD markers DHS-3::GFP (Zhang *et al.* 2012) and mRuby::DGAT-2 (Xu *et al.* 2012) further confirmed that FAC indeed increases LD size (Figure 1D). Furthermore, lipid quantitation by TLC/GC shows that the relative percentage of triacylglycerol (TAG/total lipids, %) significantly increased in N2 worms under FAC treatment (5.0 mg/ml) compared to no FAC (0 mg/ml) (Figure 1E). Since FAC at 5.0 mg/ml resulted in obvious changes of both gene expression and fat accumulation, we used this concentration in most of the subsequent experiments. The increased fat accumulation induced by FAC is not likely to be a result of citrate supplementation, since dietary supplementation of ammonium ferric sulfate (FAS) also promotes expression of FTN-1::GFP as well as fat accumulation (Figure S3). Altogether, these findings suggest that iron overload indeed concurrently promotes ferritin expression and fat accumulation.

To investigate the underlying genetic mechanisms and signaling pathways required for this synergetic effect, we performed a selective genetic screen using RNAi knockdowns as well as mutant strains corresponding to ~2000 genes, including transcription factors, kinases, cytochrome P450 family, and lipid metabolic genes. We screened RNAi knockdowns or mutations that led to changes in GFP fluorescence of the *ftn-1*::*GFP(XA6900)* strain after iron (FAC) exposure. We chose *ftn-1*, rather than *ftn-2*, because it shows the greatest response to iron in *C. elegans* (Gourley *et al.* 2003; Kim *et al.* 2004). In strains that failed to induce *ftn-1*::*GFP* after iron exposure, we further screened with Nile Red staining of fixed nematodes to determine if fat accumulation was also affected. We found that the elevated expression of FTN-1::GFP (Figure 1A) as well as *ftn-1* mRNA (Figure 1B) induced by FAC was suppressed in the *sgk-1(ok538)* mutant strain. The *sgk-1* gene encodes an ortholog of the serum and glucocorticoid-induced kinase in mammals (Hertweck *et al.* 2004). Furthermore, in the absence of FAC, compared to N2, the expression of *ftn-1* mRNA was decreased in *sgk-1(ok538)* mutant, but was increased in an integrated *sgk-1*::*gfp* (MQD862, *N2;Psgk-1*::*sgk-1*::*gfp*) strain (Figure 1B) (Hertweck *et al.* 2004; Zhu *et al.* 2015). In the presence of FAC, like in N2, the expression of *ftn-1* mRNA was increased in both gain-of-function mutant *sgk-1(ft15)* (Jones *et al.* 2009) and *sgk-1*::*gfp* (MQD862, *N2;Psgk-1*::*sgk-1*::*gfp*) worms (Figure 1B). These results indicate that *sgk-1* regulates the expression of *ftn-1*.

Interestingly, we found that both the *sgk-1(ok538)* deletion mutants as well as the *sgk-1(ft15)* gain-of-function mutants had slightly increased fat content than N2 in the absence of iron (Figure 1E), consistent with previous reports (Jones *et al.* 2009; Soukas *et al.* 2009). However, when grown on FAC, only the *sgk-1(ft15)* gain-of-function mutants showed increased fat content (Figure 1E) and LD size (Figure 1C, Figure S1, A and C, Figure S2), indicating that SGK-1 activity is necessary for the induction of fat accumulation.

Since the *sgk-1(ok538)* deletion mutant was able to suppress the elevated expression of *ftn-1* as well as the increase in fat content under iron overload, we asked whether the upregulation of *ftn-1*, as well as increased fat accumulation, were due to the induced expression of *sgk-1*. We found that FAC induced the level of *sgk-1* mRNA in N2 worms by twofold (Figure 1F) and also led to increased intensity of GFP fluoresence in *sgk-1*::*gfp* and *Psgk-1*::*gfp* worms (Figure 1G). The increased GFP fluorescence was observed using the integrated *sgk-1*::*gfp* (MQD862, *N2;Psgk-1*::*sgk-1*::*gfp*) translational fusion strain (Hertweck *et al.* 2004; Zhu *et al.* 2015) (Figure 1G, left), as well as with a transcriptional reporter containing 2.2 kb of upstream *sgk-1* promoter sequence fused to *gfp*, *Psgk-1*::*gfp* {kun*Ex*126, [*unc-119(ed3);Psgk-1*::*gfp*+*unc-119(+)*]} (Figure 1G, right). Interestingly, the two reporter strains showed different tissue expression. The translational SGK-1::GFP expresses in some head and tail neurons, with diffuse expression in the intestine (Hertweck *et al.* 2004), but the promoter-only fusion shows expression only in the intestine (Figure 1G, Figure S4), implying that the coding region of *sgk-1* may contain regulatory sequences necessary for neuronal expression. Nevertheless, FAC led to increased expression of *sgk-1* mRNA as well as increased fluorescence intensity in both strains (Figure 1, F and G), suggesting that FAC induces the transcriptional expression of *sgk-1*. Conversely, restriction of iron by BP (2,2′-bipyridyl, 0.1 mM), an iron chelator (Breuer *et al.* 1995; Romney *et al.* 2008, 2011), also represses the expression of SGK-1::GFP (MQD862, *N2;Psgk1*::*sgk-1*::*gfp*) (Figure S5). Altogether, these studies show that iron overload induces the expression of *sgk-1*, which promotes the expression of *ftn-1* and fat accumulation.

cyp-23A1 represses sgk-1 to regulate ferritin expression and fat accumulation

We identified a mutant strain, *cyp-23A1(gk253)*, predicted to carry a loss-of-function mutation in a gene encoding a member of the cytochrome P450 family, that greatly enhanced the expression of FTN-1::GFP (Figure 2A) and *ftn-1* mRNA (up to

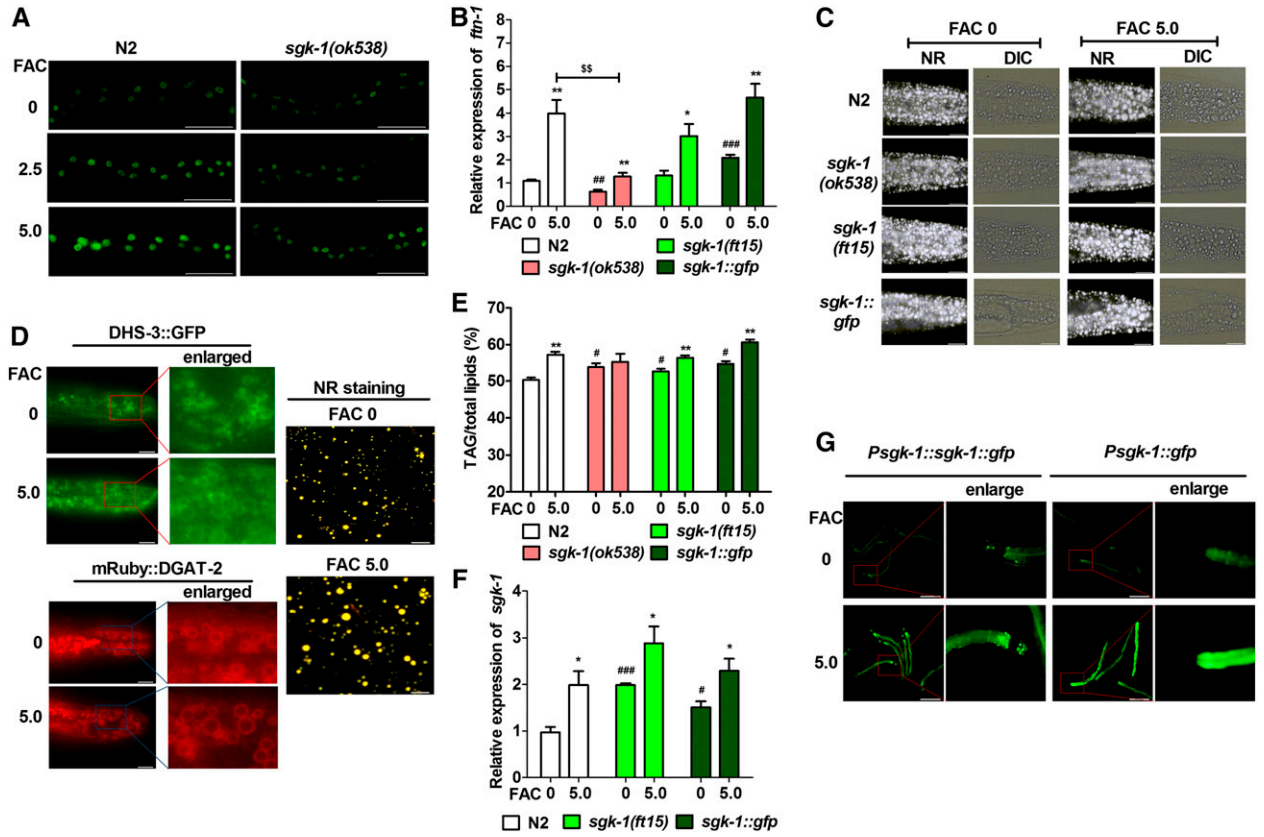

Figure 1 Iron overload induces *sgk-1* expression to upregulate ferritin expression and fat accumulation. (A) Expression of FTN-1::GFP [*XA6900(ftn-1::GFP)*]. For represented animals, anterior is left and posterior is right. Bar, 50 μm. Exposure time, 140 ms. (B) Relative expression of *ftn-1* mRNA by qPCR. Data are presented as mean ± SEM of four biological repeats. (C) Nile Red staining of fixed worms. NR, Nile Red staining; DIC, differential interference contrast microscopy. For represented animals, anterior is left and posterior is right. Bar, 20 μm. Exposure time, 25 ms. (D, left) The expression of lipid droplet markers DHS-3::GFP (top) and mRuby::DGAT-2 (bottom). Bar, 20 μm. Exposure time, 87 ms for DHS-3::GFP; 114 ms for mRuby::DGAT-2. (D, right) Isolated lipid droplets of N2 worms stained with Nile Red. Bar, 20 μm. Exposure time, 46 ms. (E) Percentage of triacylglycerol (TAG) in total lipids (TAG+PL, phospholipids) quantitated by TLC/GC. Data are presented as mean ± SEM of three biological repeats. (F) The relative expression of *sgk-1* mRNA. Data are presented as mean ± SEM of four biological repeats. (G) The expression of SGK-1::GFP. Bar, 100 μm. Exposure time, 87 ms. The selected area of a represented worm was enlarged for clear view. Significant difference between FAC treatment and no FAC in same worm strain, $^{*}P < 0.05$, $^{**}P < 0.01$. Significant difference between N2 and a specific worm strain under no FAC, $^{\#}P < 0.05$, $^{\#\#}P < 0.01$, $^{\#\#\#}P < 0.001$. Significant difference between N2 and a specific worm strain under FAC treatment, $^{\$\$}P < 0.01$.

13.6-fold) (Figure 2B) compared to N2 under FAC treatment, suggesting that CYP-23A1 activity represses ferritin expression. Since iron overload induced the expression of *sgk-1*, we asked whether the exacerbated effects in the *cyp-23A1(gk253)* mutant strain could be due to misregulation of *sgk-1*. We found that the expression of *sgk-1* mRNA (Figure 2C), as well as the intensity of the SGK-1::GFP (MQD862, *N2;Psgk1::sgk-1::gfp*) (Figure 2D), was higher in *cyp-23A1(gk253)* mutants than in N2 in both the absence and presence of FAC. In addition, Western blot analysis using anti-SGK-1 antibody also showed that the level of SGK-1 protein was significantly higher in *cyp-23A1(gk253)* mutants than in N2, both in the presence and absence of FAC (Figure 2, E and F). Remarkably, the highly induced expression of *ftn-1* mRNA (Figure 2B) as well as the increased intensity of FTN-1::GFP (Figure 2A) in the *cyp-23A1(gk253)* mutant was abolished in *sgk-1(ok538)* background. Therefore, these findings indicate that CYP-23A1 represses *sgk-1* expression, which eventually leads to decreased *ftn-1* expression.

Next, we asked whether *cyp-23A1* also affects fat accumulation. In the absence of FAC, the *cyp-23A1(gk253)* mutant displayed normal lipid droplet size similar to N2 (Figure 2G, Figure S1, A and F, Figure S2), although TLC/GC analysis revealed slightly higher fat content compared to N2 (Figure 2H). Similar to N2, iron overload increased fat accumulation (Figure 2H) and lipid droplet size (Figure 2G, Figure S1, A and F, Figure S2) in *cyp-23A1(gk253)* mutants, but was dependent on *sgk-1* since both lipid droplet size and fat content did not increase in the *sgk-1(ok538);cyp-23A1(gk253)* double mutant strain (Figure 2, G and H, Figure S1, A and G, Figure S2). Collectively, these data show that CYP-23A1 appears to repress *sgk-1* to regulate the level of ferritin and fat accumulation under iron overload.

The insulin/IGF-1 signaling pathway was previously reported to work with hypoxia signaling to regulate iron

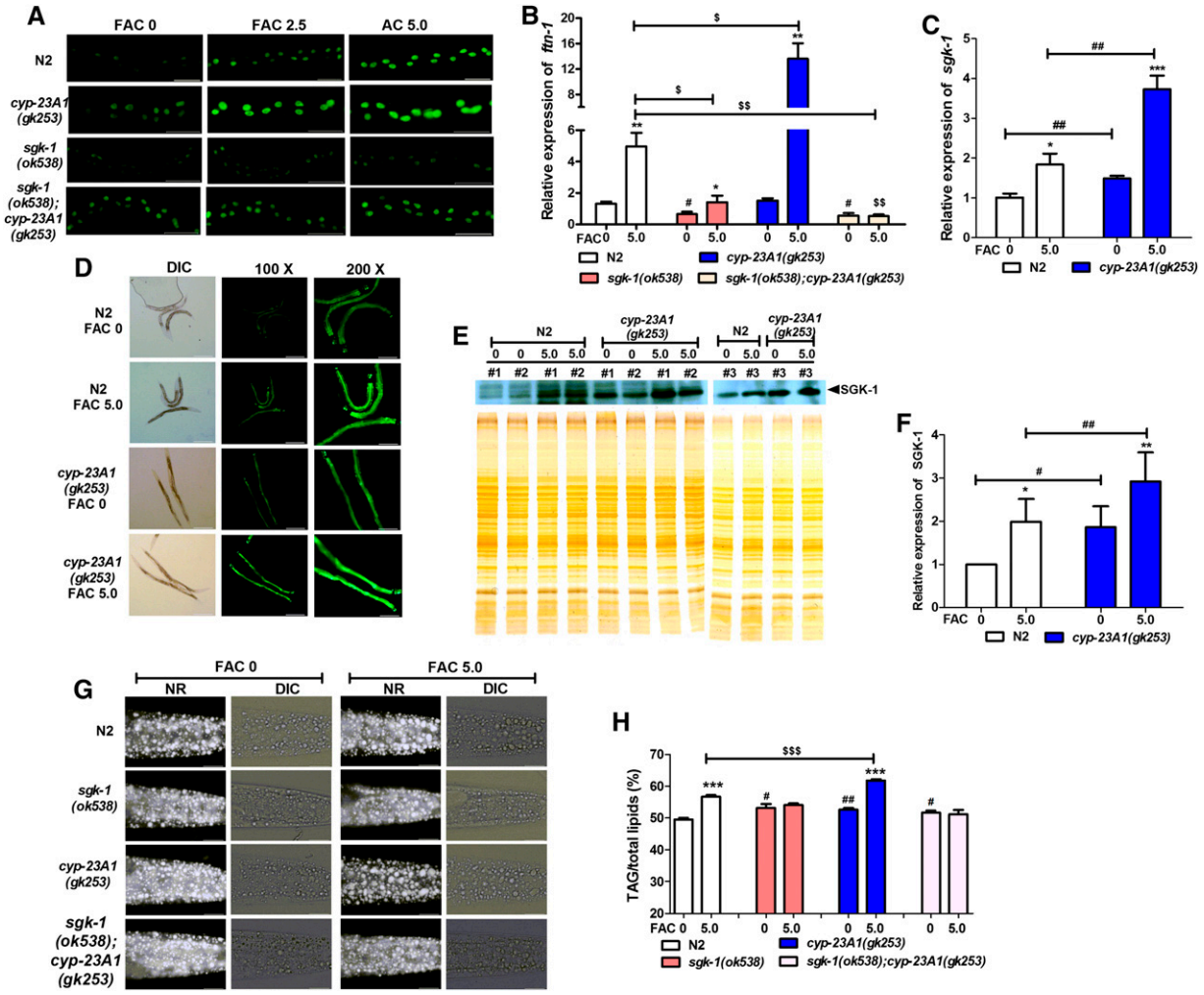

Figure 2 Expression of *sgk-1* is enhanced in *cyp-23A1(gk253)* mutants to promote ferritin expression and fat accumulation. (A) Expression of FTN-1::GFP. For represented animals, anterior is left and posterior is right. Bar, 50 μm. Exposure time, 140 ms. (B and C) Relative expression of *ftn-1* mRNA (B) and *sgk-1* mRNA (C) by qPCR. Data are presented as mean ± SEM of four biological repeats. (D) The expression of SGK-1::GFP (MQD862, *N2;Psgk1*::*sgk-1*::*gfp*). Bar, 20 μm. Exposure time, 25 ms. Magnification, 100× and 200×. (E) Western blot with anti-SGK-1 antibody (top), and silver staining of SDS-PAGE indicating equal amount of total proteins loaded (bottom). (F) Relative level of SGK-1 protein quantified with three biological repeats from E. (G) Nile Red staining of fixed worms. NR, Nile Red staining; DIC, differential interference contrast microscopy. For represented animals, anterior is left and posterior is right. Bar, 20 μm. Exposure time, 25 ms. (H) Percentage of triacylglycerol (TAG) in total lipids (TAG+PL, phospholipids) quantitated by TLC/GC. Data are presented as mean ± SEM of three or five biological repeats. Significant difference between FAC treatment and no FAC in same worm strain, $^{*}P < 0.05$, $^{**}P < 0.01$, $^{***}P < 0.001$. Significant difference between N2 and a specific worm strain under no FAC, $^{\#}P < 0.05$, $^{\#\#}P < 0.01$. Significant difference between N2 and a specific worm strain under FAC treatment, $^{\$}P < 0.01$, $^{\$\$}P < 0.05$, $^{\$\$\$}P < 0.001$.

homeostasis in *C. elegans* (Ackerman and Gems 2012). However, RNAi knockdown of two reported transcriptional factors *daf-16*, encoding the FOXO homolog in the insulin/IGF-1 signaling pathway, and *hif-1*, encoding hypoxia-inducible factor-1 (Romney *et al.* 2011; Ackerman and Gems 2012), did not suppress the expression of *ftn-1* mRNA in *cyp-23A1(gk253)* mutant background under FAC treatment, even though *cyp-23A1(gk253)* mutant successfully reversed the high expression of *ftn-1* mRNA in *hif-1*RNAi worms under no FAC (Figure S6A). Additionally, the repression of *sgk-1* expression by CYP-23A1 also appears to be independent of the transcription factors DAF-16 and HIF-1 (Figure S6B).

Iron facilitates lipid uptake via sgk-1

The capacity of lipid accumulation ultimately depends on the homeostasis of lipid synthesis, lipolysis, uptake, and transport. Previous studies contend that SGK-1 may participate in insulin/IGF-1 or target of rapamycin (TOR) signaling pathways to regulate lipid metabolism (Jones *et al.* 2009; Soukas *et al.* 2009; Lang and Stournaras 2013). However, we found that several mutants of genes in both pathways, *e.g.*, *daf-2 (e1370)*, *age-1(hx546)*, *akt-1(ok525)*, *daf-16(mu86)*, and *rsks-1(ok1255)* (Figure S7A), are responsive to iron-promoted fat accumulation, implying that they may not be directly involved in iron-induced fat accumulation. Furthermore,

our analysis shows that FAC treatment has both positive and negative effects on gene expression of both lipid synthesis and lipid degradation genes, thus it is not clear from this analysis to what extent the balance of *de novo* lipid synthesis and degradation is disrupted by FAC (Figure S8, A–C).

To test the hypothesis that iron may enhance the production of reactive oxygen species (ROS) and induce oxidative damage that may impair the function of mitochondria and lipid oxidation (Levi and Rovida 2009), we examined the expression of genes encoding superoxide dismustases, *sod-1*, *sod-2*, *sod-3*, and *sod-4*, but found no significant gene expression changes (Figure S8D). We performed dihydroethidium (DHE) staining, which is widely used to evaluate reactive oxygen species production, and observed no significant changes after FAC treatment (Figure S8E). Finally, the relative oxygen consumption rate did not differ in N2, *sgk-1(ok538)*, *cyp-23A1(gk253)*, *sgk-1(ok538); cyp-23A1(gk253)* worms between FAC treatment and no FAC (Figure S8F). Taken together, these results do not support the hypothesis that iron overload is inducing oxidative stress or increased oxygen consumption in *C. elegans*.

The yeast *Ypk1*, the ortholog of human *sgk-1*, was previously found to be required for efficient fatty acid uptake (Jacquier and Schneiter 2010). Since increased lipid accumulation by iron overload is dependent on *sgk-1*, we posited that iron-induced lipid accumulation may be due to increased lipid uptake under regulation of SGK-1. After conducting staining of BODIPY-C12 fatty acid to indicate lipid uptake in *C. elegans* (Spanier *et al.* 2009), we found that iron indeed promoted lipid uptake as more fluorescence accumulated in the whole intestine of N2, *cyp-23A1(gk253)*, *sgk-1(ft15)* worms at FAC 5.0 mg/ml compared to control (FAC 0 mg/ml) (Figure 3, A and B). However, in the *sgk-1(ok538)* and *sgk-1(ok538);cyp-23A1(gk253)* worms, fluorescence of BODIPY-C12 did not increase with FAC concentration (Figure 3A), which was mostly aggregated in the intestinal lumen, suggesting that iron-promoted lipid uptake depends on SGK-1.

To confirm these results, we further supplemented the *C. elegans* diet with OA, [C18:1(n-9), 0.2 mM]. Consistent with our previously report (Shi *et al.* 2013), *C. elegans* incorporated C18:1(n-9) in all six tested strains in the absence of iron (Figure 3, C and D). Additionally, iron overload enhanced an even higher level of C18:1(n-9) in N2, *sgk-1*::*gfp* (MQD862, *N2;Psgk-1*::*sgk-1*::*gfp*), and *sgk-1(ft15)* worms than under no FAC (Figure 3, C and D), further confirming that iron facilitates lipid uptake. Consistent with the results of dietary BODIPY-C12, under iron overload the level of C18:1 (n-9) dramatically increased in *cyp-23A1(gk253)* worms, but remained unchanged in the *sgk-1(ok538)* mutant background (Figure 3C). Thus, dietary supplementation of BODIPY-C12 fatty acid and uptake of oleic acid support our hypothesis that SGK-1 is required for lipid uptake under iron overload.

The fatty acid transporter ACS-20 is required for iron-induced lipid uptake

The observation that iron overload facilitates lipid uptake to promote lipid accumulation raised the question of which gene products are responsible for lipid uptake in response to FAC. Generally, dietary lipids are taken up by cells by lipid transporters. The *C. elegans* genome contains a number of genes with homology to known lipid transporters that may display similar or distinct functions (Zhang *et al.* 2013). We tested several strains with mutations in putative lipid transporter genes including the *acs-20(tm3232)* strain, which carries a deletion in the *acs-20* gene that encodes an ortholog of mammalian fatty acid transport proteins FATP1/4 (Kage-Nakadai *et al.* 2010) (www.wormbase.org). We found that lipid droplet size (Figure S1, A and H), fat storage indicated by postfix Nile Red staining (Figure 4A) and LipidTox Red staining (Figure S2), as well as quantitated by TLC/GC (Figure 4B), were unchanged in the *acs-20(tm3232)* mutants compared to N2 after iron overload. Thus, *acs-20* is necessary for iron-promoted fat accumulation.

We next investigated whether the increased fat accumulation was due to activated *acs-20*. The expression of *acs-20* mRNA was slightly, but significantly, increased in N2 at FAC 2.5 mg/ml (Figure 4C). However, at FAC 5.0 mg/ml, the relative expression of *acs-20* mRNA was significantly increased to 3.9-fold in *cyp-23A1(gk253)* mutants compared to N2 (Figure 4C). Meanwhile, the increased expression of *acs-20* in both N2 and *cyp-23A1(gk253)* mutant was significantly reduced in *sgk-1(ok538)* mutant background (Figure 4C), while the *acs-20(tm3232);cyp-23A1(gk253)* double mutants showed no response to iron-induced fat accumulation (Figure 4, A and D, Figure S2) and increased LD size (Figure S1, A and I). These findings suggest that *sgk-1* upregulates *acs-20* to promote fat accumulation under iron overload.

We then tested whether ACS-20 accounts for fatty acid transport under iron overload. Dietary supplement with BODIPY-C12 fatty acid showed that the fluorescence did not obviously increase with FAC concentration at 5.0 mg/ml in *acs-20(tm3232)* single and *acs-20(tm3232);cyp-23A1(gk253)* double mutants, unlike in N2 and the *cyp-23A1(gk253)* mutants (Figure 4E). Consistent with this finding, dietary supplementation of C18:1(n-9) further confirmed that unlike N2 and *cyp-23A1(gk253)* mutants, both *acs-20(tm3232)* and *acs-20(tm3232);cyp-23A1(gk253)* worms did not displayed increased levels of C18:1(n-9) in response to iron overload (Figure 4F), suggesting that the *acs-20* mutants significantly suppressed the increased fatty acid uptake in both N2 and *cyp-23A1(gk253)* mutants. These results further confirmed that the fatty acid transporter ACS-20 accounts for iron facilitated lipid uptake under SGK-1 regulation.

VIT-2 translocates dietary lipids to lipid droplets

When taken up into cells, lipids are translocated into intracellular organelles for further utilization or storage in lipid

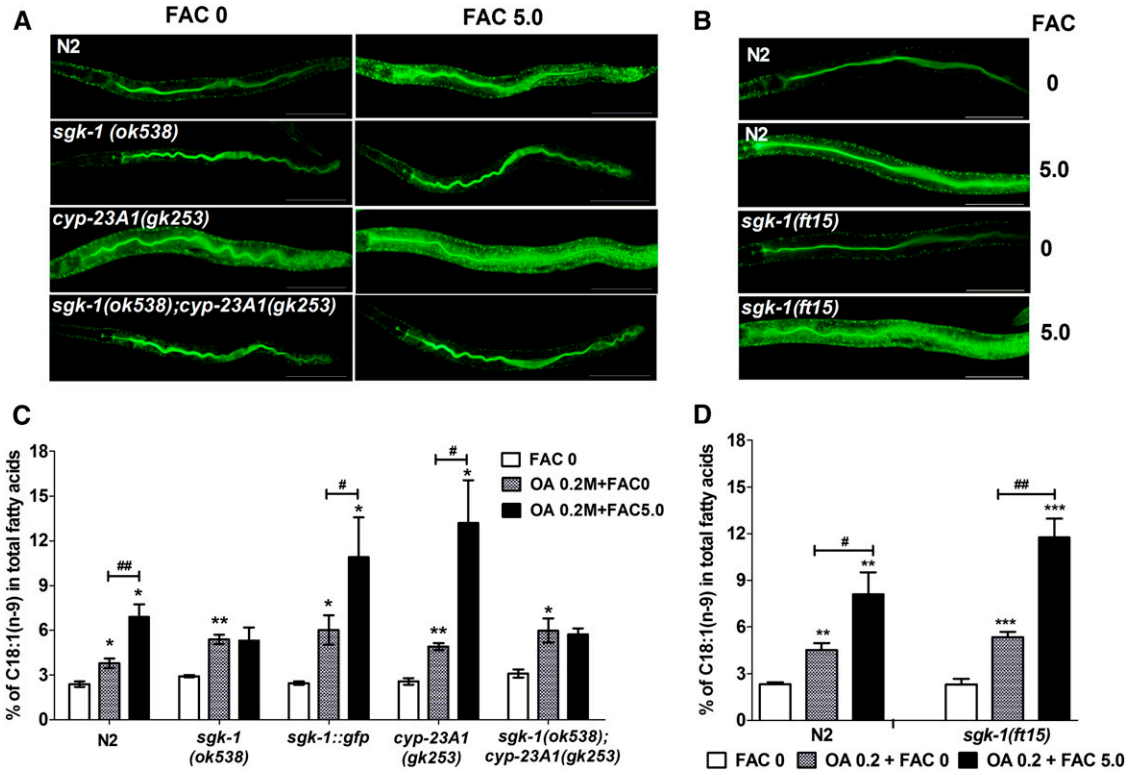

Figure 3 Iron facilitates lipid uptake. (A and B) BODIPY C-12 staining. For represented animals, anterior is left and posterior is right. At least 30 worms were observed for each genotype. Bar, 100 μm. Exposure time, 20 ms. (C and D) Dietary supplementation with oleic acid [OA, C18:1(n-9)] with or without FAC treatment. Data are presented as mean ± SEM of four to five biological repeats. Significant difference between OA treatment and no OA in same worm strain, $^{*}P < 0.05$, $^{**}P < 0.01$, $^{***}P < 0.001$. Significant difference between FAC treatment and no FAC in same worm strain, $^{\#}P < 0.05$, $^{\#\#}P < 0.01$.

droplets. As mentioned above, iron overload promotes lipid uptake for storage. We hypothesized that intracellular lipid transporters may be necessary to translocate lipids to lipid droplets for storage, so we searched for such an intracellular lipid transporter under iron overload. *C. elegans* genome contains six genes, *vit-1–6*, predicted to encode vitollogenins, which are homologous to the protein moieties of mammalian lipoproteins such as LDL (Baker 1988), which may have intracellular as well as intercellular lipid transport activity (Spieth and Blumenthal 1985; MacMorris *et al.* 1994; Grant and Hirsh 1999). We found that the relative mRNA expression of *vit-2* and *vit-3* transcripts was almost undetectable in *sgk-1(ok538)* mutant compared to N2, even under iron overload (Figure 5A). Meanwhile, we crossed the *vit-2*::*gfp* (RT130, *pwIs23*) transgenic strain into *sgk-1(ok538)* mutant, and found that VIT-2::GFP was undetectable by fluorescent microscopy. These results indicate that *sgk-1* positively regulates the expression of *vit-2* and *vit-3*.

Next, we treated *vit-2*::*gfp* (RT130, *pwIs23*) worms with FAC and found that the fluorescent intensity of VIT-2::GFP (Figure 5B) and the expression level of VIT-2 protein (Figure 5C) was markedly increased at FAC 5.0 mg/ml as compared to the control. The expression of VIT-2::GFP is also brighter in *cyp-23A1(gk253)* mutant, but not in *acs-20(tm3232)* mutant compared to N2 under both FAC treatment and no FAC (Figure S9). VIT-2 is a yolk lipoprotein, but it has also been reported to be a *C. elegans* lipid droplet-associated protein (Zhang *et al.* 2012; Vrablik *et al.* 2015). After isolating lipid droplets and other cellular fractions of *vit-2*::*gfp* worms treated with FAC 0 and 5.0 mg/ml, Western blot analysis using anti-GFP antibody showed that the level of VIT-2 protein was significantly increased in LD, total membrane (TM), and postnuclear supernatant (PNS) under FAC 5.0 mg/ml compared to FAC 0 mg/ml (Figure 5, D and E). Taken together, these results demonstrated that iron overload activates the expression of VIT-2, and this may promote lipid translocation to lipid droplets.

Since iron overload was able to activate the SGK-1-dependent expression of *vit-2* and *vit-3* (Figure 5A), we consequently hypothesized that worms depleted of *vit-2* or *vit-3* might be resistant to iron overload, similar to *sgk-1(ok538)* mutants. Indeed, compared to N2, lipid abundance did not increase in *vit-2(ok3211)* or *vit-3(ok2348)* mutants (Figure 5, F and G, Figure S2) in response to iron overload. Additionally, unlike N2, the lipid droplet size of *vit-2(ok3211)* did not change under iron overload (Figure 5H, Figure S1, A and J). However, both *vit-2(ok3211)* and *vit-3(ok2348)* mutant still displayed increased level of oleic acid [C18:1(n-9)] (Figure 5I). Taken together, these results

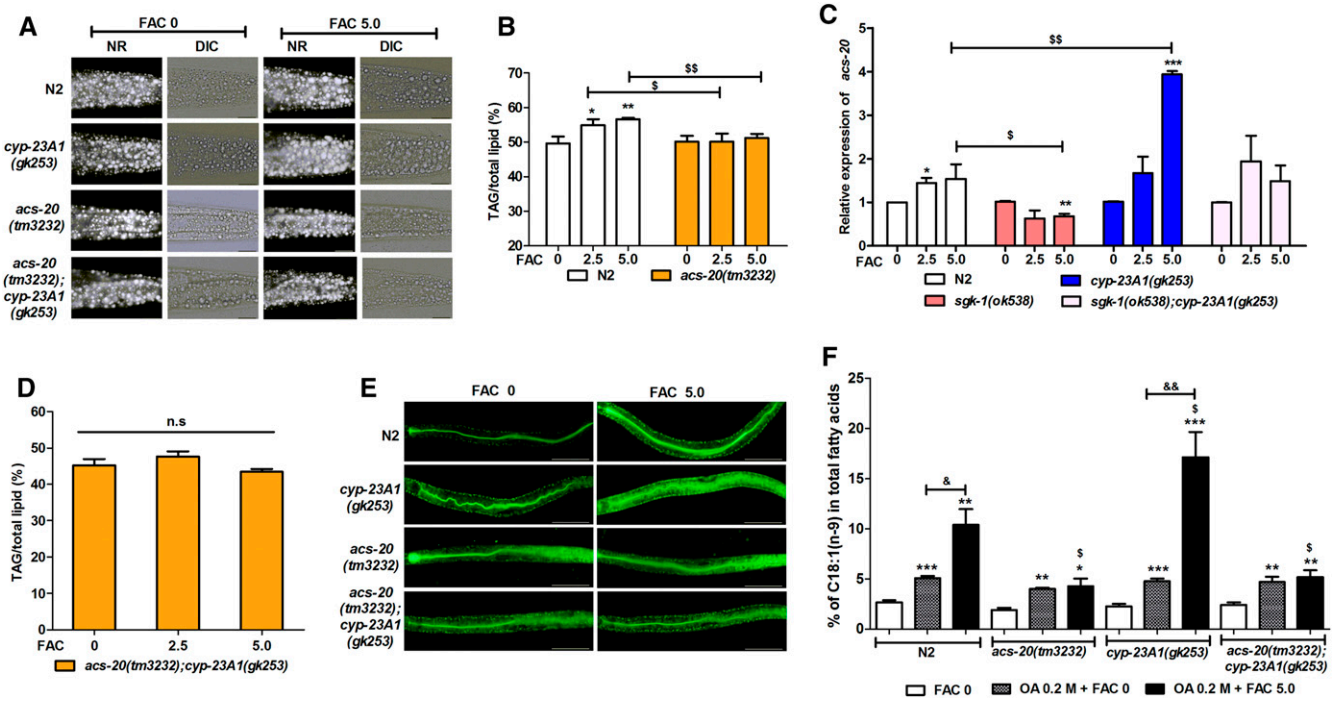

Figure 4 ACS-20 is required for iron-induced lipid uptake. (A) Nile Red staining of fixed worms. NR, Nile Red staining; DIC, differential interference contrast microscopy. For represented animals, anterior is left and posterior is right. Bar, 20 μm. Exposure time, 25 ms. (B and D) Percentage of triacylglycerol (TAG) in total lipids (TAG+PL, phospholipids) quantitated by TLC/GC. Data are presented as mean ± SEM of three biological repeats. (C) Relative expression of *acs-20* mRNA by qPCR. Data are presented as mean ± SEM of three biological repeats. (E) BODIPY C-12 staining. For represented animals, anterior is left and posterior is right. Bar, 100 μm. Exposure time, 20 ms. (F) Dietary supplementation with OA [C18:1(n-9)]. Data are presented as mean ± SEM of four to six biological repeats. Significant difference between treatment (FAC/OA) and no treatment (FAC 0) in same worm strain, $^{*}P < 0.05$, $^{**}P < 0.01$, $^{***}P < 0.001$. Significant difference between N2 and a specific worm strain under same treatment, $^{\$}P < 0.05$, $^{\$\$}P < 0.01$. Significant difference between FAC treatment and no FAC treatment in same worm strain, $^{\&}P < 0.05$, $^{\&\&}P < 0.01$. n.s., no significance.

suggest that VIT-2/3 may function to transport dietary lipids to lipid droplets for storage in response to iron.

Discussion

The correlation between iron overload and obesity is not mechanistically understood. Using a genetic screen to reveal genes required for the induction of ferritin as well as changes in lipid metabolism upon exposure to iron overload, we found that the serum and glucocorticoid-inducible kinase SGK-1 plays a central role to synergistically regulate iron and lipid homeostasis.

SGK1 belongs to the family of AGC kinases, is regulated by numerous different factors, and participates in a variety of cellular and physiological processes (Lang *et al.* 2009; Lang and Stournaras 2013). The transcriptional expression of SGK-1 has been previously reported to be downregulated by iron restriction in rat intestine (Marzullo *et al.* 2004) and kidney of chronic kidney disease in a rat model (Naito *et al.* 2012). Here, we consistently observed that iron restriction by the iron cheater BP represses the expression of SGK-1::GFP (MQD862, *N2;Psgk1*::*sgk-1*::*gfp*) in *C. elegans* (Figure S5). Meanwhile, iron overload induces expression of both the transcriptional and translational SGK-1::GFP reporters (Figure 1G), as well as the level of *sgk-1* mRNA (Figure 1F, Figure 2C) and protein (Figure 2, E and F) in N2 and in *cyp-23A1* mutants. Additionally, the *sgk-1(ok538)* mutation successfully suppressed the induced expression of ferritin in both N2 and in the *cyp-23A1(gk253)* mutants. Our present findings, along with work by others, offer consistent evidence of an evolutionarily conserved function of SGK-1 in response to iron to regulate iron homeostasis.

In mammals, SGK-1 has been implicated into glucose and lipid metabolism, as well as several metabolic diseases (Lang *et al.* 2009; Lang and Stournaras 2013). A common SGK1 gene variant is associated with increased blood pressure, obesity, and type 2 diabetes (Schwab *et al.* 2008). Upregulation of intestinal SGK1 expression may partially stimulate the Na^{+}-coupled glucose transporter SGLT1, consequently leading to fat deposition and obesity (Fujita *et al.* 1998; Dieter *et al.* 2004; Lang and Stournaras 2013). SGK1 is expressed in white adipose tissue and its levels are induced during the conversion of preadipocytes into fat cells by direct phosphorylation of Foxo1 (Di Pietro *et al.* 2010). In *C. elegans*, several reports showed that SGK-1 regulates development, stress response, longevity, lipid metabolism (Hertweck *et al.* 2004; Jones *et al.* 2009; Soukas *et al.* 2009), and more recently, membrane trafficking (Zhu *et al.* 2015). Here we show that the gain-of-function mutant *sgk-1(ft15)* (Figure 1F), *sgk-1*::*gfp* (MQD862, *N2;Psgk-1*::

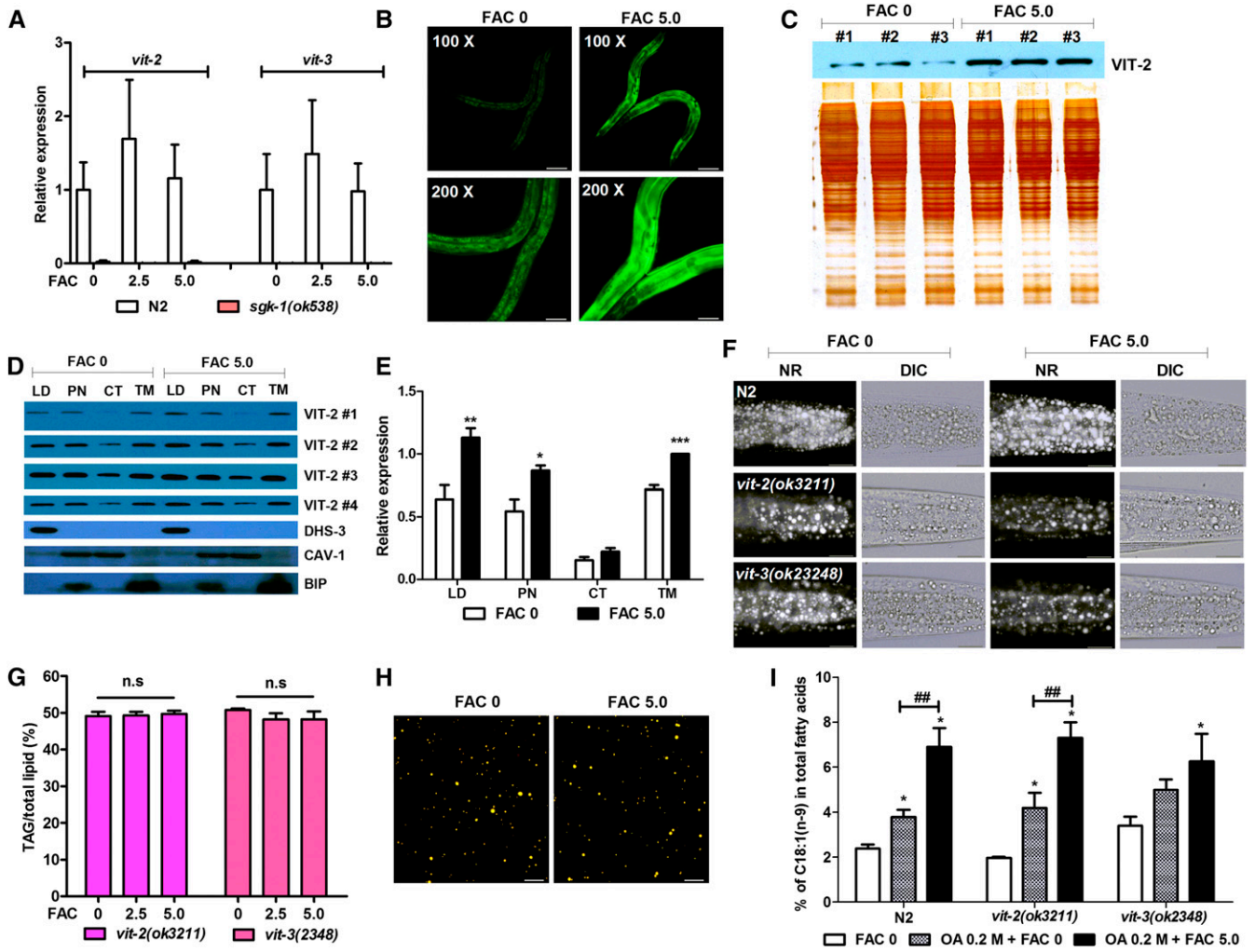

Figure 5 Iron overload induces VIT-2 expression to transport lipids for storage. (A) Relative expression of *vit-2* and *vit-3* mRNA. Data are presented as mean ± SEM of three biological repeats. (B) Expression of VIT-2::GFP. Bar, 100 μm. Exposure time, 334 ms. Magnification, 100× and 200×. (C and D) The expression level of VIT-2 in total proteins (C) and in different fractions (D). (C) Western blot analysis of *vit-2*::*gfp* (RT130, pwIs23) worms with anti-GFP antibody (top) and silver staining of SDS-PAGE, indicating equal amount of total proteins loaded (bottom). One to four biological repeats are shown. (D) LD proteins and proteins from other cellular fractions (lipid droplets, LD; total membrane, TM; cytosol, CT; PNS, postnuclear supernatant) were confirmed by cellular organelle markers: LD marker, DHS-3; PN and TM marker, CAV-1; endoplasmic reticulum (ER) marker, Bip/GRP78. (E) Relative level of VIT-2 protein quantified with three biological repeats from D. The level of VIT-2 protein in TM under FAC 5.0 was used as standard. (F) Nile Red staining of fixed worms. For represented animals, anterior is left and posterior is right. NR: Nile Red staining; DIC, differential interference contrast microscopy. Bar, 20 μm. Exposure time, 25 ms. (G) Percentage of triacylglycerol (TAG) in total lipids (TAG+PL, phospholipids) quantitated by TLC/GC. (H) Isolate lipid droplets of *vit-2(ok3211)* worms on FAC 0 and 5.0 mg/ml. (I) Dietary supplementation with OA [C18:1(n-9)]. All data are presented as mean ± SEM of three biological repeats. Significant difference between FAC/OA treatment and no treatment in same worm strain, $^{*}P < 0.05$, $^{**}P < 0.01$. Significant difference between FAC treatment and no FAC in same worm strain, $^{\#\#}P < 0.01$. n.s., no significance.

sgk-1::*gfp*) (Figure 1F), and *cyp-23A1(gk253)* mutants (Figure 2C) displayed increased expression of *sgk-1* and correspondingly higher fat content than wild-type N2 in both the absence and the presence of iron. These findings provide strong evidence that SGK-1 plays a crucial role in regulating lipid metabolism from *C. elegans* to mammals, which in turn further supports the usefulness of *C. elegans* to serve as a model to investigate the role of *sgk-1* in lipid metabolism.

Lipid uptake and translocation are known to require lipid transporters. The *C. elegans* genome contains 22 genes known to encode acyl-CoA synthetase/fatty acid transporter (Zhang *et al.* 2013), of which ACS-20 is required for incorporation of exogenous very long chain fatty acids into sphingomyelin (Kage-Nakadai *et al.* 2010). While ACS-22 may functionally overlap with ACS-20 (Kage-Nakadai *et al.* 2010), we found that only ACS-20 is required for the increased fat accumulation under iron overload, suggesting that ACS-20, like SGK-1, regulates lipid hemostasis under iron overload. Our results also showed that iron has the ability to induce the transcriptional expression of *acs-20*, especially in *cyp-23A1(gk253)* mutants (Figure 4C). Interestingly, the increased expression of *acs-20* mRNA in N2 and *cyp-23A1(gk253)* mutants was positively correlated to the

high absorption of BODIPY-C12 fatty acid and oleic acid [C18:1(n-9)] (Figure 4F). In contrast, the *acs-20(tm3232)* mutants dramatically repressed the highly increased fat accumulation (Figure 4, B and D) as well as lipid uptake (Figure 4F) of both N2 and the *cyp-23A1(gk253)* mutant. These findings strongly suggest that ACS-20 may function as fatty acid transport to uptake lipids to store under iron overload. Since the increased expression of *acs-20* in both N2 and *cyp-23A1(gk253)* mutant relied on *sgk-1*, we further propose that iron induces the expression of *sgk-1*, which in turn further activates *acs-20* expression to uptake lipid into intestine for storage (Figure 6). This process may also explain the uncharacterized function of yeast Ypk1 in the regulation of fatty acid uptake, though clearly more follow-up is needed for confirmation.

C. elegans vit-1–6 belong to the family of vitellogenin genes that encode the protein moiety of yolk lipoproteins (Spieth and Blumenthal 1985; MacMorris *et al.* 1994; Grant and Hirsh 1999). While previous work has shown that yolk lipoproteins are synthesized in the intestine and transferred to developing oocytes using receptor-mediated endocytosis (Grant and Hirsh 1999), the roles of lipoproteins in intracellular lipid transfer have not previously been characterized. In our study, we found that *vit-2* and *vit-3* expression were dramatically repressed in the *sgk-1(ok538)* mutants (Figure 5A), indicating that SGK-1 is required for normal expression of vitellogenin genes. Furthermore, we found that *vit-2(ok3211)* and *vit-3(ok2348)* mutants were not responsive to iron-induced fat accumulation (Figure 5, F and G, Figure S2). Although the reduced fat accumulation may be due to reduced yolk production, an alternative interpretation is that vitellogenins play a role in intracellular lipid transport. VIT-2 was recently identified as a lipid droplet-associated protein (Zhang *et al.* 2012; Vrablik *et al.* 2015), and here we found that iron promoted the accumulation of VIT-2 protein in LDs (Figure 5, D and E). Meanwhile, the expression of VIT-2::GFP is also brighter in *cyp-23A1(gk253)* mutant, but not in *acs-20(tm3232)* mutants compared to N2 regardless of treatment with FAC (Figure S9). However, unlike the *sgk-1(ok538)* and *acs-20(tm3232)* mutants, the *vit-2(ok3211)* mutants still responded to iron-promoted oleic acid uptake (Figure 5I), suggesting that VIT-2 may function as a lipid transporter to facilitate intracellular lipid translocation to lipid droplets for storage under conditions of iron overload.

Cytochromes P450 are hemoproteins containing a heme cofactor and are known to be involved in numerous processes, such as lipid metabolism and detoxification (Pikuleva and Waterman 2013). Within 77 of 81 tested cytochrome P450 genes, we found that only *cyp-23A1*, like *sgk-1*, synergistically, but oppositely, regulated iron and lipid metabolism. CYP-23A1 is a homolog of the human gene CYP7B1 (Kuwabara and O'Neil 2001), which hydroxylates carbons 6 and 7 of the B-ring of oxysterols and steroids (Stiles *et al.* 2009). Mutations in the *CYP7B1* gene are a cause of neonatal hemochromatosis (OMIM:231100) (Jimenez-Sanchez *et al.* 2001), characterized by hepatic failure in the newborn period and heavy iron staining in the liver. Remarkably, the *C. elegans cyp-23A1(gk253)* mutant also consistently displayed high expression of FTN-1::GFP and *ftn-1* mRNA under iron overload, indicating CYP23A1, like CYP7B1, has an evolutionarily conserved role regulating iron homeostasis. Interestingly, *sgk-1(ok538)* mutants successfully suppressed the highly elevated expression of FTN-1::GFP and *ftn-1* mRNA, as well as fat accumulation in the *cyp-23A1(gk253)* mutants under iron overload, which may offer a new approach to investigate *CYP7B1*-related diseases.

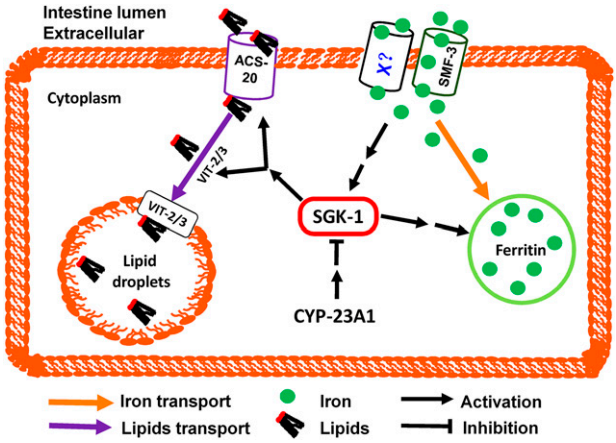

Figure 6 A model of how SGK-1 response to iron to synergistically regulate iron and lipid homeostasis. Iron is taken up by SMF-3 and uncharacterized factor X into the cell. Iron uptake induces the expression of *sgk-1*, which is indirectly repressed by CYP-23A1, to facilitate lipid uptake and translocation for storage via fatty acid transporter ACS-20 and vitellogenin VIT-2/3. SGK-1 also positively regulates ferritin and iron homeostasis. X, uncharacterized factor(s).

In summary, this study indicates that iron overload has the capacity to synergistically upregulate the level of ferritin and fat accumulation in an intact organism, *C. elegans*, thereby offering experimental evidence supporting a previously unverified link between iron and obesity. Although more research is necessary to elucidate all of the molecular mechanisms that participate in this complex process, by taking the advantage of genetics in *C. elegans*, we were able to characterize a novel response to iron overload, which induces the expression of *sgk-1* to facilitate lipid uptake via fatty acid transporter ACS-20, and to translocate fats to lipid droplets for storage via VIT-2/3 (Figure 6). In this pathway, SGK-1 plays a central role in coordinating the regulation of ferritin levels and lipid accumulation in response to iron overload. Since SGK1 knockout mice display no obvious physiological defects (Wulff *et al.* 2002), targeting of SGK1 may hold promise in treating diseases related to iron and lipid metabolism.

Acknowledgments

We express our deep gratitude to Jennifer L. Watts for helpful comments on the manuscript; Mengqiu Dong for kindly providing the *sgk-1*::*gfp* (MQD862, *N2;Psgk1*::*sgk-1*::*gfp*)

worm strain; and Shouhong Guang for EG4322, pCFJ151, pJL43.1, pCFJ104, and pCFJ90 constructs. Some strains were provided by the *Caenorhabditis* Genetics Center, which is funded by the National Institutes of Health Office of Research Infrastructure Programs (P40 OD010440). This work was supported by the Strategic Priority Research Program of the Chinese Academy of Sciences (XDB13030600), the National Natural Science Foundation of China (31460268, 31160216, 31171134, and U1202223), the Yunnan Natural Science Foundation (2013FA042 and 2011FZ179), the Yunnan Provincial Science and Technology Department (2014HB022), the Yunnan Overseas High-Level Talents Program (2015HA040 to B.L.), and the State Key Laboratory of Genetic Resources and Evolution (GREKF13-03).

Author contributions: B.L., H.W., X.Z., and X.J. conceived and designed the experiments, H.W., X.J., X.Z., J.W., L.Z., and Y.Z. performed the experiments; B.L., H.W., X.J., and X.Z. analyzed the data; H.W., X.J., L.Z., X.Z., J.H., and B.L. contributed reagents/materials/analysis tools; and B.L., H.W., and X.Z. wrote the paper. The authors declare that they have no competing interests.

Literature Cited

Ackerman, D., and D. Gems, 2012 Insulin/IGF-1 and hypoxia signaling act in concert to regulate iron homeostasis in Caenorhabditis elegans. PLoS Genet. 8: e1002498.

Anderson, C. P., and E. A. Leibold, 2014 Mechanisms of iron metabolism in Caenorhabditis elegans. Front. Pharmacol. 5: 113.

Baker, M. E., 1988 Is vitellogenin an ancestor of apolipoprotein B-100 of human low-density lipoprotein and human lipoprotein lipase? Biochem. J. 255: 1057–1060.

Bozzini, C., D. Girelli, O. Olivieri, N. Martinelli, A. Bassi *et al.*, 2005 Prevalence of body iron excess in the metabolic syndrome. Diabetes Care 28: 2061–2063.

Breuer, W., S. Epsztejn, and Z. I. Cabantchik, 1995 Iron acquired from transferrin by K562 cells is delivered into a cytoplasmic pool of chelatable iron(II). J. Biol. Chem. 270: 24209–24215.

Brooks, K. K., B. Liang, and J. L. Watts, 2009 The influence of bacterial diet on fat storage in C. elegans. PLoS One 4: e7545.

Choi, J. S., I. U. Koh, H. J. Lee, W. H. Kim, and J. Song, 2013 Effects of excess dietary iron and fat on glucose and lipid metabolism. J. Nutr. Biochem. 24: 1634–1644.

Cook, J. D., D. A. Lipschitz, L. E. Miles, and C. A. Finch, 1974 Serum ferritin as a measure of iron stores in normal subjects. Am. J. Clin. Nutr. 27: 681–687.

Di Pietro, N., V. Panel, S. Hayes, A. Bagattin, S. Meruvu *et al.*, 2010 Serum- and glucocorticoid-inducible kinase 1 (SGK1) regulates adipocyte differentiation via forkhead box O1. Mol. Endocrinol. 24: 370–380.

Dieter, M., M. Palmada, J. Rajamanickam, A. Aydin, A. Busjahn *et al.*, 2004 Regulation of glucose transporter SGLT1 by ubiquitin ligase Nedd4–2 and kinases SGK1, SGK3, and PKB. Obes. Res. 12: 862–870.

Ding, Y., X. Zou, X. Jiang, J. Wu, Y. Zhang *et al.*, 2015 Pu-erh tea down-regulates sterol regulatory element-binding protein and stearyol-CoA desaturase to reduce fat storage in Caenorhaditis elegans. PLoS One 10: e0113815.

Dongiovanni, P., A. L. Fracanzani, S. Fargion, and L. Valenti, 2011 Iron in fatty liver and in the metabolic syndrome: a promising therapeutic target. J. Hepatol. 55: 920–932.

Fleming, R. E., and P. Ponka, 2012 Iron overload in human disease. N. Engl. J. Med. 366: 348–359.

Frokjaer-Jensen, C., M. W. Davis, C. E. Hopkins, B. J. Newman, J. M. Thummel *et al.*, 2008 Single-copy insertion of transgenes in Caenorhabditis elegans. Nat. Genet. 40: 1375–1383.

Fujita, Y., H. Kojima, H. Hidaka, M. Fujimiya, A. Kashiwagi *et al.*, 1998 Increased intestinal glucose absorption and postprandial hyperglycaemia at the early step of glucose intolerance in Otsuka Long-Evans Tokushima Fatty rats. Diabetologia 41: 1459–1466.

Gillum, R. F., 2001 Association of serum ferritin and indices of body fat distribution and obesity in Mexican American men: the Third National Health and Nutrition Examination Survey. Int. J. Obes. Relat. Metab. Disord. 25: 639–645.

Gourley, B. L., S. B. Parker, B. J. Jones, K. B. Zumbrennen, and E. A. Leibold, 2003 Cytosolic aconitase and ferritin are regulated by iron in Caenorhabditis elegans. J. Biol. Chem. 278: 3227–3234.

Graham, R. M., A. C. Chua, K. W. Carter, R. D. Delima, D. Johnstone *et al.*, 2010 Hepatic iron loading in mice increases cholesterol biosynthesis. Hepatology 52: 462–471.

Grant, B., and D. Hirsh, 1999 Receptor-mediated endocytosis in the Caenorhabditis elegans oocyte. Mol. Biol. Cell 10: 4311–4326.

Hertweck, M., C. Gobel, and R. Baumeister, 2004 C. elegans SGK-1 is the critical component in the Akt/PKB kinase complex to control stress response and life span. Dev. Cell 6: 577–588.

Hubler, M. J., K. R. Peterson, and A. H. Hasty, 2015 Iron homeostasis: A new job for macrophages in adipose tissue? Trends Endocrinol. Metab. 26: 101–109.

Iwasaki, T., A. Nakajima, M. Yoneda, Y. Yamada, K. Mukasa *et al.*, 2005 Serum ferritin is associated with visceral fat area and subcutaneous fat area. Diabetes Care 28: 2486–2491.

Jacquier, N., and R. Schneiter, 2010 Ypk1, the yeast orthologue of the human serum- and glucocorticoid-induced kinase, is required for efficient uptake of fatty acids. J. Cell Sci. 123: 2218–2227.

Jehn, M., J. M. Clark, and E. Guallar, 2004 Serum ferritin and risk of the metabolic syndrome in U.S. adults. Diabetes Care 27: 2422–2428.

Jimenez-Sanchez, G., B. Childs, and D. Valle, 2001 Human disease genes. Nature 409: 853–855.

Jones, K. T., E. R. Greer, D. Pearce, and K. Ashrafi, 2009 Rictor/TORC2 regulates Caenorhabditis elegans fat storage, body size, and development through sgk-1. PLoS Biol. 7: e60.

Kage-Nakadai, E., H. Kobuna, M. Kimura, K. Gengyo-Ando, T. Inoue *et al.*, 2010 Two very long chain fatty acid acyl-CoA synthetase genes, acs-20 and acs-22, have roles in the cuticle surface barrier in Caenorhabditis elegans. PLoS One 5: e8857.

Kim, C. H., H. K. Kim, S. J. Bae, J. Y. Park, and K. U. Lee, 2011 Association of elevated serum ferritin concentration with insulin resistance and impaired glucose metabolism in Korean men and women. Metabolism 60: 414–420.

Kim, Y. I., J. H. Cho, O. J. Yoo, and J. Ahnn, 2004 Transcriptional regulation and life-span modulation of cytosolic aconitase and ferritin genes in C. elegans. J. Mol. Biol. 342: 421–433.

Kuwabara, P. E., and N. O'Neil, 2001 The use of functional genomics in C. elegans for studying human development and disease. J. Inherit. Metab. Dis. 24: 127–138.

Lang, F., and C. Stournaras, 2013 Serum and glucocorticoid inducible kinase, metabolic syndrome, inflammation, and tumor growth. Hormones (Athens) 12: 160–171.

Lang, F., A. Gorlach, and V. Vallon, 2009 Targeting SGK1 in diabetes. Expert Opin. Ther. Targets 13: 1303–1311.

Levi, S., and E. Rovida, 2009 The role of iron in mitochondrial function. Biochim. Biophys. Acta 1790: 629–636.
Liang, B., K. Ferguson, L. Kadyk, and J. L. Watts, 2010 The role of nuclear receptor NHR-64 in fat storage regulation in Caenorhabditis elegans. PLoS One 5: e9869.
MacMorris, M., J. Spieth, C. Madej, K. Lea, and T. Blumenthal, 1994 Analysis of the VPE sequences in the Caenorhabditis elegans vit-2 promoter with extrachromosomal tandem array-containing transgenic strains. Mol. Cell. Biol. 14: 484–491.
Marzullo, L., A. Tosco, R. Capone, H. S. Andersen, A. Capasso *et al.*, 2004 Identification of dietary copper- and iron-regulated genes in rat intestine. Gene 338: 225–233.
Mascitelli, L., F. Pezzetta, and M. R. Goldstein, 2009 Iron, metabolic syndrome, nonalcoholic fatty liver disease and carotid atherosclerosis. Atherosclerosis 205: 39–40.
Moreno-Navarrete, J. M., F. Ortega, M. Moreno, W. Ricart, and J. M. Fernandez-Real, 2014a Fine-tuned iron availability is essential to achieve optimal adipocyte differentiation and mitochondrial biogenesis. Diabetologia 57: 1957–1967.
Moreno-Navarrete, J. M., F. Ortega, M. Moreno, M. Serrano, W. Ricart *et al.*, 2014b Lactoferrin gene knockdown leads to similar effects to iron chelation in human adipocytes. J. Cell. Mol. Med. 18: 391–395.
Naito, Y., A. Fujii, H. Sawada, S. Hirotani, T. Iwasaku *et al.*, 2012 Effect of iron restriction on renal damage and mineralocorticoid receptor signaling in a rat model of chronic kidney disease. J. Hypertens. 30: 2192–2201.
Nikonorov, A. A., M. G. Skalnaya, A. A. Tinkov, and A. V. Skalny, 2015 Mutual interaction between iron homeostasis and obesity pathogenesis. J. Trace Elem. Med. Biol. 30C: 207–214.
Pikuleva, I. A., and M. R. Waterman, 2013 Cytochromes p450: roles in diseases. J. Biol. Chem. 288: 17091–17098.
Romney, S. J., C. Thacker, and E. A. Leibold, 2008 An iron enhancer element in the FTN-1 gene directs iron-dependent expression in Caenorhabditis elegans intestine. J. Biol. Chem. 283: 716–725.
Romney, S. J., B. S. Newman, C. Thacker, and E. A. Leibold, 2011 HIF-1 regulates iron homeostasis in Caenorhabditis elegans by activation and inhibition of genes involved in iron uptake and storage. PLoS Genet. 7: e1002394.
Rumberger, J. M., T. Peters, Jr., C. Burrington, and A. Green, 2004 Transferrin and iron contribute to the lipolytic effect of serum in isolated adipocytes. Diabetes 53: 2535–2541.
Schwab, M., A. Lupescu, M. Mota, E. Mota, A. Frey *et al.*, 2008 Association of SGK1 gene polymorphisms with type 2 diabetes. Cell. Physiol. Biochem. 21: 151–160.
Shi, X., J. Li, X. Zou, J. Greggain, S. V. Rodkaer *et al.*, 2013 Regulation of lipid droplet size and phospholipid composition by stearoyl-CoA desaturase. J. Lipid Res. 54: 2504–2514.
Soukas, A. A., E. A. Kane, C. E. Carr, J. A. Melo, and G. Ruvkun, 2009 Rictor/TORC2 regulates fat metabolism, feeding, growth, and life span in Caenorhabditis elegans. Genes Dev. 23: 496–511.
Spanier, B., K. Lasch, S. Marsch, J. Benner, W. Liao *et al.*, 2009 How the intestinal peptide transporter PEPT-1 contributes to an obesity phenotype in Caenorhabditits elegans. PLoS One 4: e6279.
Spieth, J., and T. Blumenthal, 1985 The Caenorhabditis elegans vitellogenin gene family includes a gene encoding a distantly related protein. Mol. Cell. Biol. 5: 2495–2501.
Stiles, A. R., J. G. McDonald, D. R. Bauman, and D. W. Russell, 2009 CYP7B1: one cytochrome P450, two human genetic diseases, and multiple physiological functions. J. Biol. Chem. 284: 28485–28489.
Tajima, S., Y. Ikeda, K. Sawada, N. Yamano, Y. Horinouchi *et al.*, 2012 Iron reduction by deferoxamine leads to amelioration of adiposity via the regulation of oxidative stress and inflammation in obese and type 2 diabetes KKAy mice. Am. J. Physiol. Endocrinol. Metab. 302: E77–E86.
Tinkov, A. A., V. S. Polyakova, and A. A. Nikonorov, 2013 Chronic administration of iron and copper potentiates adipogenic effect of high fat diet in Wistar rats. Biometals 26: 447–463.
Valentini, S., F. Cabreiro, D. Ackerman, M. M. Alam, M. B. Kunze *et al.*, 2012 Manipulation of in vivo iron levels can alter resistance to oxidative stress without affecting ageing in the nematode C. elegans. Mech. Ageing Dev. 133: 282–290.
Van Rompay, L., C. Borghgraef, I. Beets, J. Caers, and L. Temmerman, 2015 New genetic regulators question relevance of abundant yolk protein production in C. elegans. Sci. Rep. 5: 16381.
Vrablik, T. L., V. A. Petyuk, E. M. Larson, R. D. Smith, and J. L. Watts, 2015 Lipidomic and proteomic analysis of Caenorhabditis elegans lipid droplets and identification of ACS-4 as a lipid droplet-associated protein. Biochim. Biophys. Acta 1851: 1337–1345.
Watts, J. L., and J. Browse, 2002 Genetic dissection of polyunsaturated fatty acid synthesis in Caenorhabditis elegans. Proc. Natl. Acad. Sci. USA 99: 5854–5859.
Watts, J. L., and J. Browse, 2006 Dietary manipulation implicates lipid signaling in the regulation of germ cell maintenance in C. elegans. Dev. Biol. 292: 381–392.
Wenzel, B. J., H. B. Stults, and J. Mayer, 1962 Hypoferraemia in obese adolescents. Lancet 2: 327–328.
Wulff, P., V. Vallon, D. Y. Huang, H. Volkl, F. Yu *et al.*, 2002 Impaired renal Na(+) retention in the sgk1-knockout mouse. J. Clin. Invest. 110: 1263–1268.
Xu, N., S. O. Zhang, R. A. Cole, S. A. McKinney, F. Guo *et al.*, 2012 The FATP1-DGAT2 complex facilitates lipid droplet expansion at the ER-lipid droplet interface. J. Cell Biol. 198: 895–911.
Zafon, C., A. Lecube, and R. Simo, 2010 Iron in obesity. An ancient micronutrient for a modern disease. Obes. Rev. 11: 322–328.
Zhang, J., R. M. Lewis, C. Wang, N. Hales, and C. D. Byrne, 2005 Maternal dietary iron restriction modulates hepatic lipid metabolism in the fetuses. Am. J. Physiol. Regul. Integr. Comp. Physiol. 288: R104–R111.
Zhang, P., H. Na, Z. Liu, S. Zhang, P. Xue *et al.*, 2012 Proteomic study and marker protein identification of Caenorhabditis elegans lipid droplets. Mol. Cell. Proteomics 11: 317–328.
Zhang, Y., X. Zou, Y. Ding, H. Wang, X. Wu *et al.*, 2013 Comparative genomics and functional study of lipid metabolic genes in Caenorhabditis elegans. BMC Genomics 14: 164.
Zhu, M., G. Wu, Y. X. Li, J. K. Stevens, C. X. Fan *et al.*, 2015 Serum- and glucocorticoid-inducible kinase-1 (SGK-1) plays a role in membrane trafficking in Caenorhabditis elegans. PLoS One 10: e0130778.
Zimmermann, M. B., 2008 Methods to assess iron and iodine status. Br. J. Nutr. 99(Suppl 3): S2–S9.

Communicating editor: O. Cohen-Fix

GENETICS

Supporting Information
www.genetics.org/lookup/suppl/doi:10.1534/genetics.116.186742/-/DC1

Iron Overload Coordinately Promotes Ferritin Expression and Fat Accumulation in *Caenorhabditis elegans*

Haizhen Wang, Xue Jiang, Jieyu Wu, Linqiang Zhang, Jingfei Huang, Yuru Zhang, Xiaoju Zou, and Bin Liang

Copyright © 2016 by the Genetics Society of America
DOI: 10.1534/genetics.116.186742

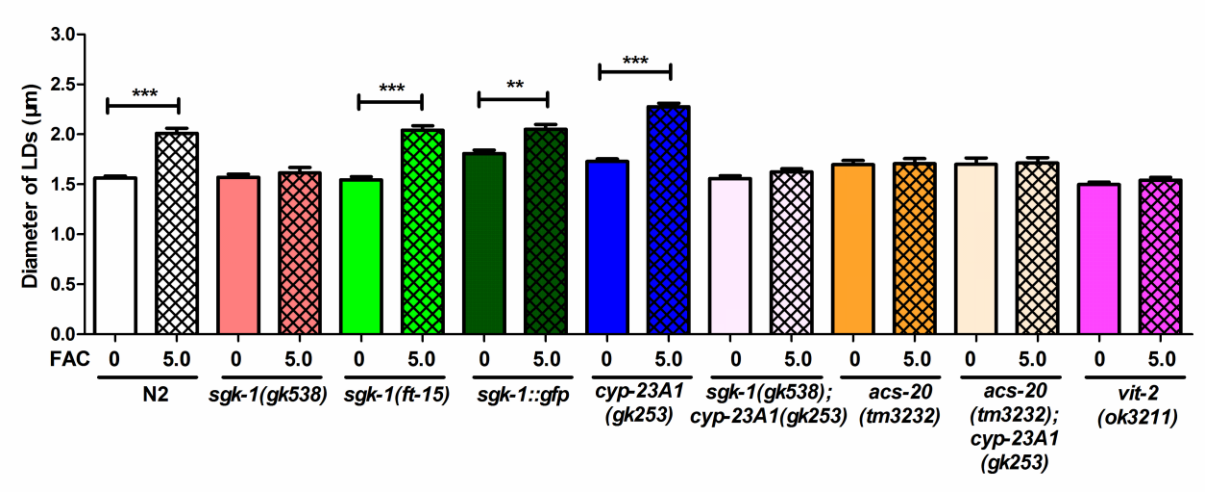

Fig. S1. Lipid droplet size and distribution. (A) The average size of lipid droplets (LDs) visualized by Nile Red staining of 5 to 6 fixed worms. (B-J) The distribution of LD size. N2 (B), *sgk1(ft15)* (C), *sgk-1::gfp* (MQD862, *N2;Psgk-1::sgk-1::gfp*) (D), *sgk-1(ok538)* (E), *cyp-23A1(gk253)* (F), *sgk-1(ok538);cyp-23A1(gk253)* (G), *acs-20(tm3232)* (H), *acs-20(tm3232);cyp-23A1(gk253)* (I), *vit-2(ok3211)* (J). Significant difference between FAC treatment and no FAC in same worm strain, **: P<0.01, ***: P<0.001.

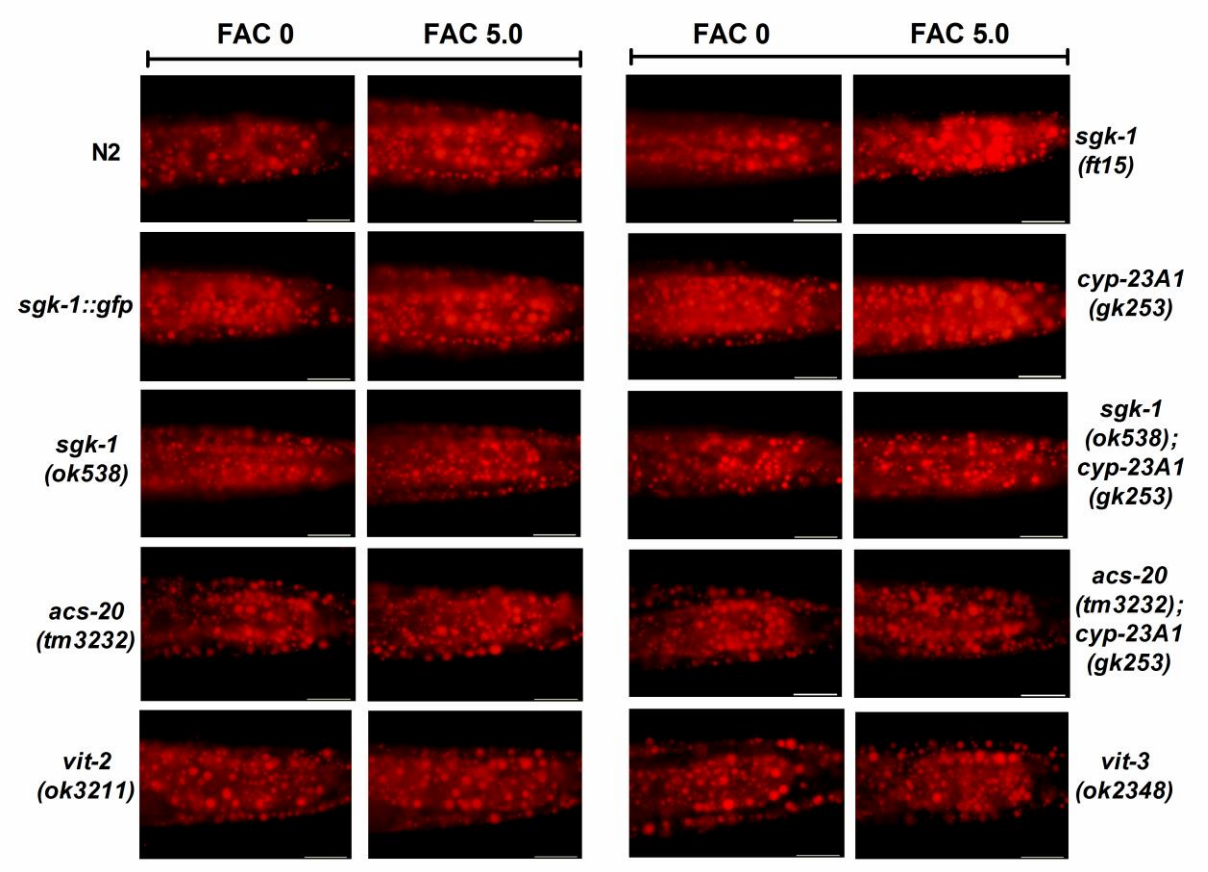

Fig. S2. LipidTox Red staining of fixed worms. Represented animals, anterior is on left, and posterior is on right. Scale bar represents 20 um. Exposure time: 120 ms. N2, *sgk-1(ft15), sgk-1::gfp* (MQD862, *N2;Psgk-1::sgk-1::gfp*), *sgk-1(ok538), cyp-23A1(gk253), sgk-1(ok538);cyp-23A1(gk253), acs-20(tm3232), acs-20(tm3232);cyp-23A1(gk253), vit-2(ok3211), vit-3(ok2348).*

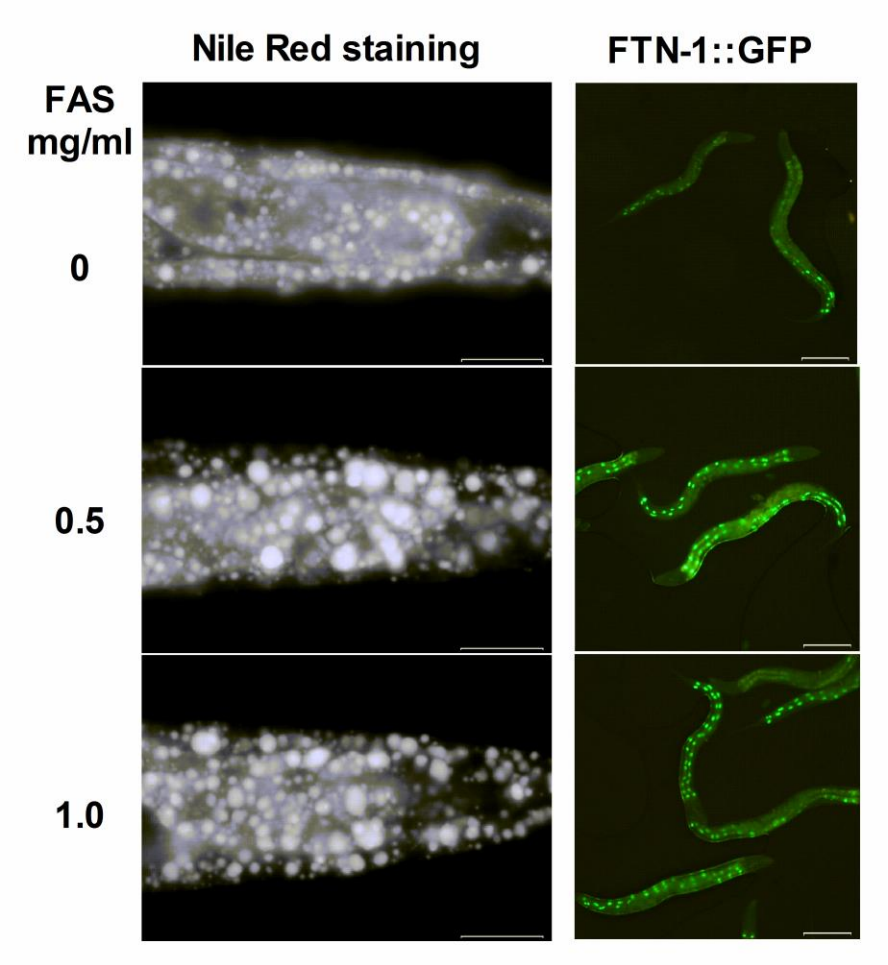

Fig. S3. Ammonium ferric sulfate (FAS) treatment. Left panels: Nile Red staining of fixed N2 worm treated with FAS [$NH_4Fe(SO_4)_2.12H_2O$]. Represented animals, anterior is on left, and posterior is on right. Scale bar represents 20 um. Exposure time: 25 ms. Right panels: Expression of FTN-1::GFP [*XA6900(ftn-1::GFP)]* under FAS condition. Scale bar represents 50 um. Exposure time: 140 ms.

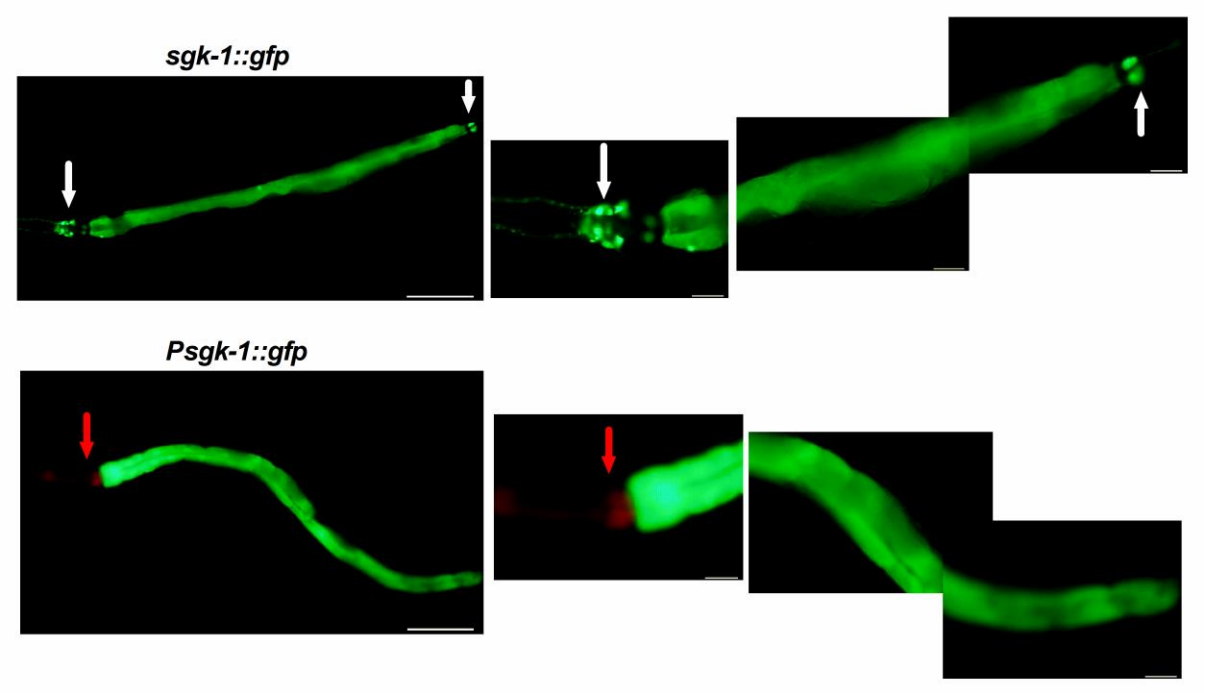

Fig. S4. The SGK-1::GFP expression patterns in *sgk-1::gfp* (MQD862, *N2;Psgk-1::sgk-1::gfp*) and *Psgk-1::gfp* {kun*Ex*126, [*unc-119(ed3);Psgk-1::gfp*+ *unc-119*(+)]} strains. Left panel: scale bar represents 100 um, exposure time was 90 ms for *sgk-1::gfp* worms (top) and 50 ms for *Psgk-1::gfp* worms (bottom). Right panel: scale bar represents 20 um. White arrows indicate head and tail neurons in *sgk-1::gfp* worm, red arrows indicate the transgenic maker mCherry in *Psgk-1::gfp* worm.

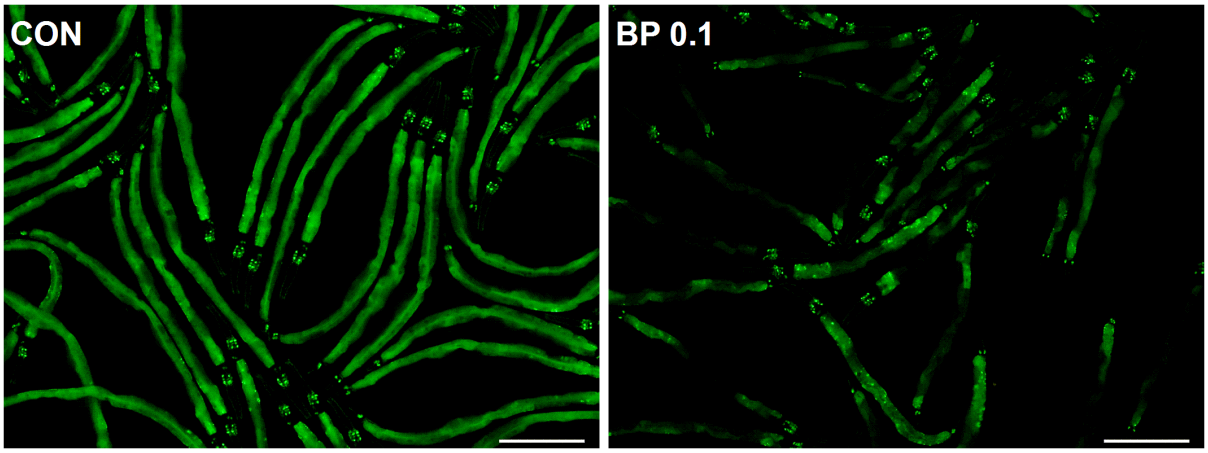

Fig. S5. The expression of SGK-1::GFP (MQD862, *N2;Psgk-1::sgk-1::gfp*) under BP (2,2'.-Bipyridyl, 0.1 mM) treatment. Scale bar represents 50 um. Exposure time: 87 ms.

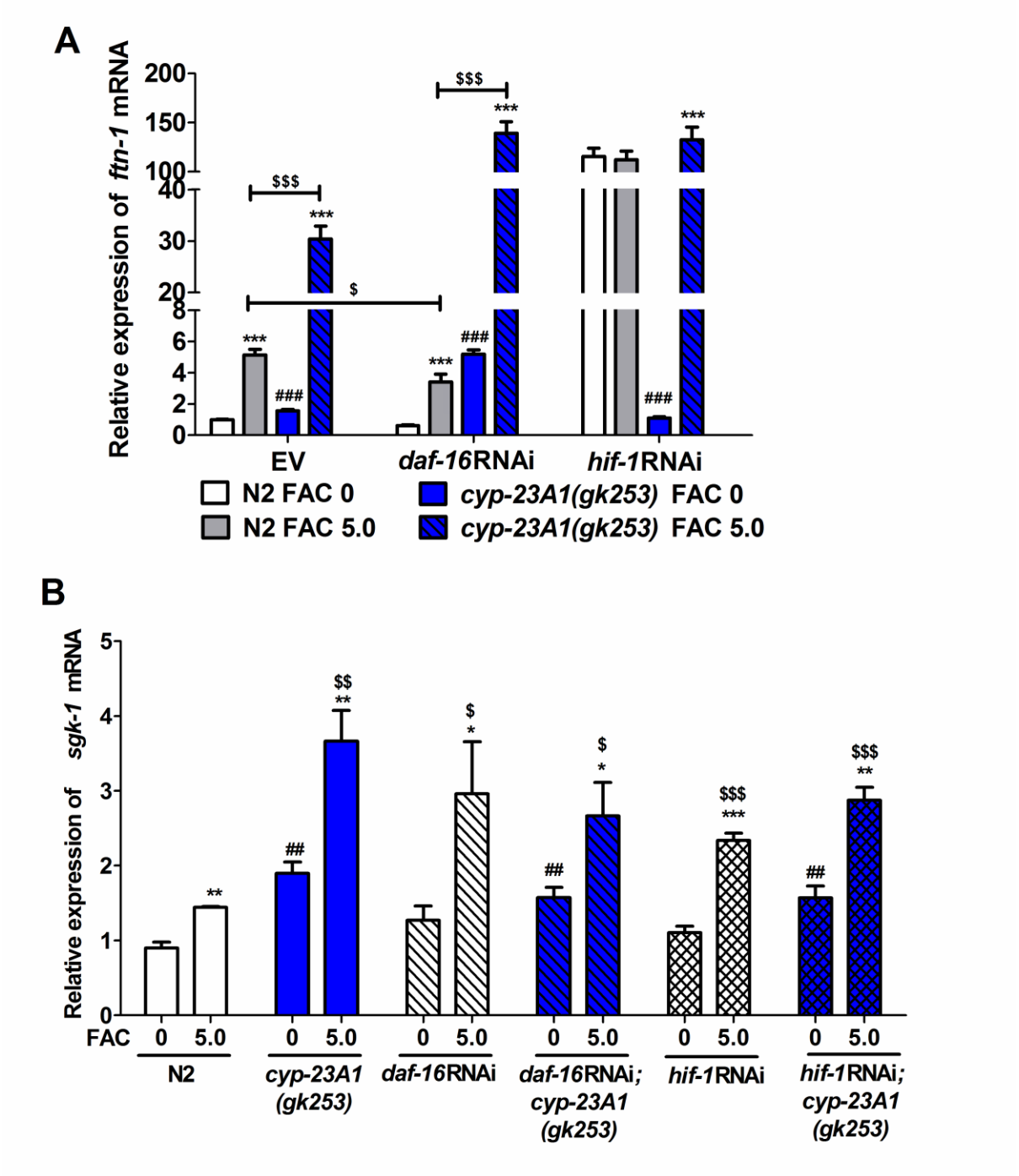

Fig. S6. The relative expression of *ftn-1* mRNA and *sgk-1* mRNA in *daf-16*RNAi and *hif-1*RNAi worms. (A) Relative expression of *ftn-1* mRNA. Data are presented as mean ± SEM of

8 biological repeats. **(B) Relative expression of *sgk-1* mRNA.** Data are presented as mean ± SEM of 4 biological repeats. Significant difference between FAC treatment and no FAC in same worm strain, *: P<0.05, **: P<0.01, ***: P<0.001. Significant difference between N2 and a specific worm strain under no FAC, ##: P<0.01, ###: P<0.001. Significant difference between N2 and a specific worm strain under FAC treatment, $: P<0.05, $$: P<0.01, $$$: P<0.001.

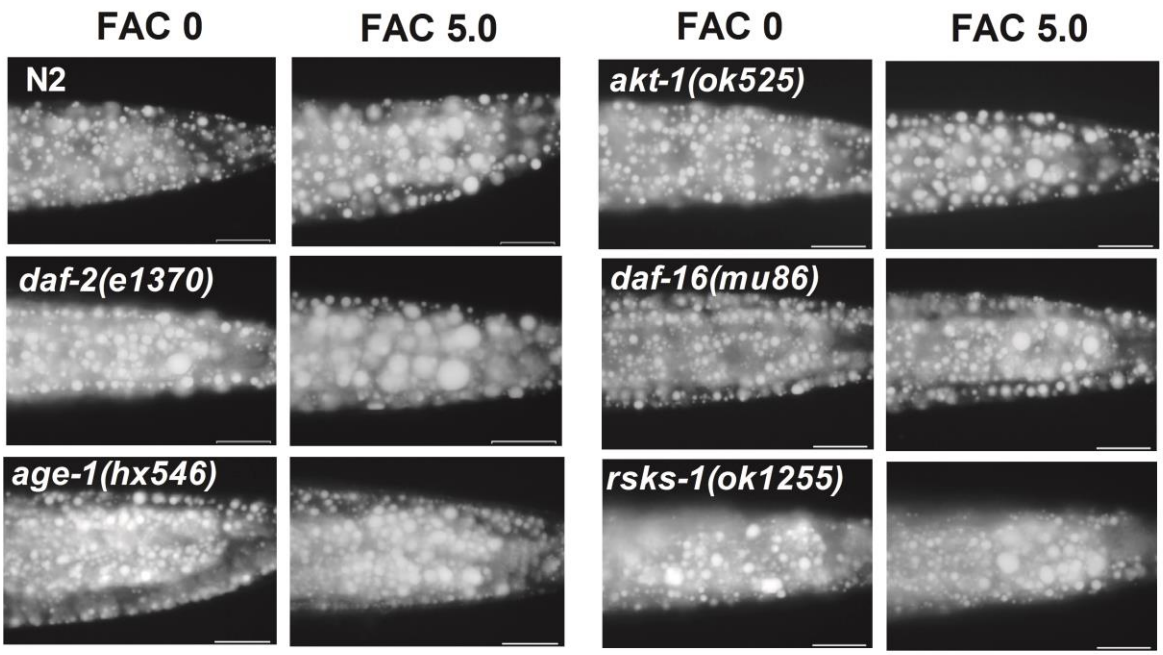

Fig. S7. FAC treatment on genes involved in insulin/IGF-1 or target of rapamycin (TOR) signaling pathways. Nile Red staining of fixed mutant worms. Represented animals, anterior is on left, and posterior is on right. Scale bar represents 20 um. Exposure time: 25 ms.

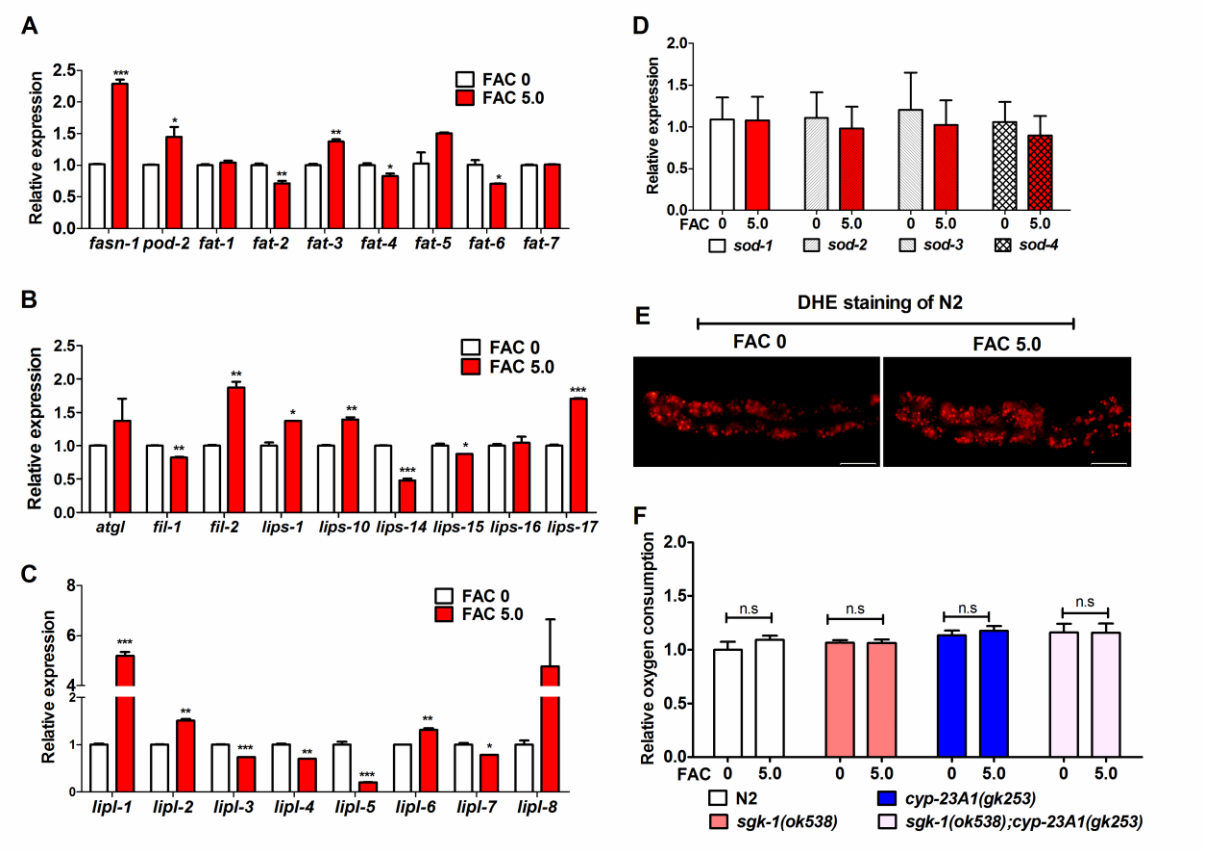

Fig. S8. The expression of lipid metabolic genes and mitochondria function. The relative expression of genes involve into fatty acids synthesis (A) and lipolysis (B and C) in N2 worms under iron overload condition. (D) The relative expression of *sod-1, sod-2, sod-3* and *sod-4* in N2 worms under FAC treatments. (E) Dihydroethidium (DHE) staining of N2 worms under FAC treatments. Represented animals, anterior is on left, and posterior is on right. Scale bar represents 20 um. Exposure time: 150 ms. (F) Relative oxygen consumption in N2, *sgk-1(ok538), cyp-23A1(gk253), sgk-1(ok538);cyp-23A1(gk253)* worms. Data are presented as mean ± SEM of 3 biological repeats. Significant difference between FAC 5.0 mg/ml and FAC 0 mg/ml in same worm strain, *: P<0.05, **: P<0.01, ***: P<0.001. n.s, no significance.

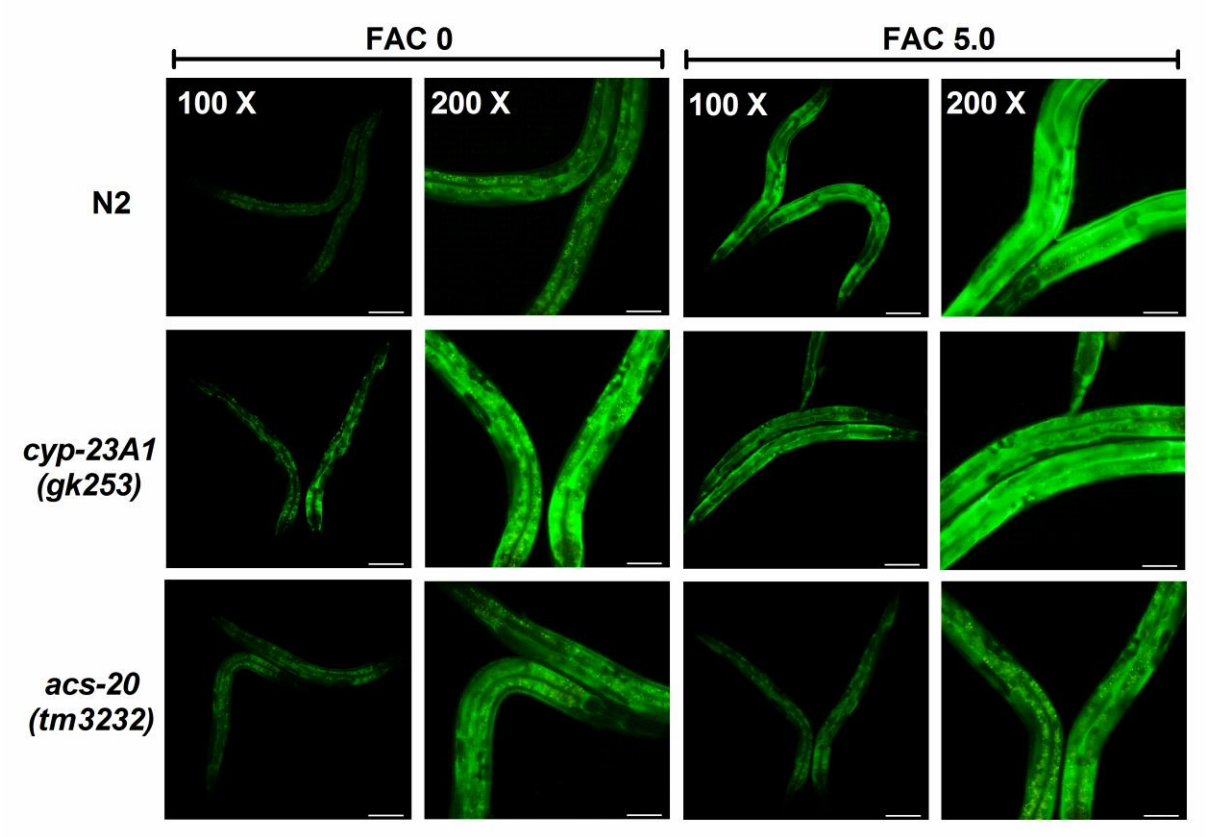

Fig. S9. The expression of VIT-2::GFP in N2, *cyp-23A1(gk253)*, and *acs-20(tm3232)* worms. Represented animals. Scale bar represents 100 um. Exposure time: 334 ms. 100 X is 100 magnifications, and 200 X is 200 magnifications.